A Novel Approach to Reaction Modeling for Photocatalytic Oxidation Processes

---

By

Clarissa Gravelle

Supervisor

Dr. Siamak Elyasi

This thesis is submitted in partial fulfillment of the requirements for the degree of

MASTER OF SCIENCE in Environmental Engineering

Faculty of Engineering

Lakehead University, Thunder Bay, Ontario, Canada

Abstract

Volatile organic compounds (VOCs) are one of the major concerns for indoor air quality. A new method for treating VOCs in the air is through an advance oxidation process (AOP) known as photocatalytic oxidation (PCO). This method uses Ultraviolet (UV) radiant power to activate the surface of a catalyst (e.g. TiO2). From the past experimental work that has been done, it can be concluded that PCO reactions follow the Langmuir-Hinshelwood (L-H) kinetic model. However, the complexity of the L-H kinetic model is difficult to simulate using existing Computation Fluid Dynamic (CFD) software. In this thesis, a new method for modeling the L-H surface reaction kinetics is proposed. The focus of this work is on the development of a novel approach to model the complex surface reaction rate expressions in order to define PCO reaction rates on the photocatalyst surfaces.

A new approach is developed to adapt the overall experimental reaction rates, which are in terms of the total system volume. This adaptation will help in deriving the actual rate of reaction happening on the catalyst surface in terms of catalyst surface area. Two cases were studied in order to demonstrate how this new approach can be used to accurately model the complex reaction kinetics of PCO systems. In each case, an integrated CFD model was developed to accurately predict the rate of VOC decomposition based on the work conducted by Shiraishi et al., (2005b) and Brosillon et al., (2008). In the first case, the experimental kinetic model for formaldehyde decomposition was adapted in order to describe a surface reaction based on formaldehyde concentration on the catalyst surface using three different approaches. It was determined that a two part polynomial rate expression was the most accurate one, as it was able to account for the higher initial rate of reaction. However, the exponential model did give reasonable results as well. In the second case, the reaction rate model was able to predict the rate of decomposition for butyric acid in the air for a variety of initial concentrations and UV irradiance levels at the catalyst surface. The developed CFD model results also discredited the assumptions made in a number of published papers that UV irradiance levels are uniform across

a catalyst surface. Finally, a simple case study was developed in order to demonstrate how the novel approach to reaction modeling could be used to predict PCO system performance treating air in a close system. In this case, the PCO system was capable of treating air contaminated with butyric acid, as well as quickly reducing the concentration below the odor threshold.

Acknowledgements

I would first like to thank my supervisor Dr. Siamak Elyasi for giving me the opportunity to pursue my Master degree. This thesis work would not have been possible without his constant support and guidance along the way and his wealth of knowledge in the field of CFD and UDF code development.

I would also like to extend a thank you to the entire Chemical Engineering Department for their guidance and support throughout my time here at Lakehead. I would also like to thank my thesis examiners Dr. Baoqiang Liao and Dr. Sam Salem for their time and efforts.

I would also like to acknowledge my fellow graduate students for their support and advice throughout these past two years. In particular, I would like to thank Jeff Hoi for his assistance in understanding the basics of building the CFD models during the initial stages of my work.

Finally, I would like to thank my family who has been there to support me in every step of the way. You have been the basis of my support system since day one and have always been there to encourage me in the pursuit of my dreams.

Table of Contents

List of Figures

List of Tables

Chapter 1 – Introduction

1.1 Introduction

Volatile organic compounds (VOCs) are defined as any organic compound with a high vapor pressure at room temperature. This can include aldehydes, alkanes, aromatics, chlorinated organic compounds, acetyls, ketones, and ethers (Cooper & Alley, 2011). VOCs are listed as primary pollutants due to the fact that they are emitted from a wide range of sources and can have a major impact on indoor air quality (IAQ).

VOCs are released from a variety of sources, such as building materials, pressed woods, paints, carpets, vinyl flooring, insulations, and adhesives, as well from household items, such as cleaning solvents, cosmetics, hair sprays, candles, tobacco smoke, and the human body (Cooper & Alley, 2011; Hodgson et al., 2002; Kagi et al., 2009). There have been a number of studies that tested the emission rates of various VOCs in different settings (Hodgson et al., 2002; Shin & Jo, 2012). Hodgson et al., (2002) looked at VOC emission rates from different building materials for new homes. They tested a wide range of wood products and found that plywood subfloors had the highest emission rates for VOCs of all the wood products tested. It was also found that softwood products have higher emission rates for VOCs (around 3 $\mu g/m^2$- h) than hardwood products. Shin and Jo (2012) looked at VOC emission rates in new apartments at the preoccupancy stage in order to determine the overall emission rates for 40 common VOCs. They found that 7 VOCs had measurable emission rates, with toluene being the largest (138 $\mu g/m^2/h$). The other VOCs (1-propanol, formaldehyde, and 2-butanone) all had emission rates below 20 $\mu g/m^2/h$. Similar to Hodgson et al., (2002) they found that wood products (mainly wood panels) were the main source of VOC emissions within apartments. Other major sources of VOCs include vinyl and other flooring, wall coverings, adhesives, and paints.

Overall, wood products appear to have the highest emission rates of VOCs within homes and office buildings compared to the other sources. This could be due to UV irradiation from sunlight reacting with the wood products to release VOCs, which was shown in a study by Kagi et al., (2009). Kagi et al., (2009) studied the effects of ozone and UV irradiation from sunlight on different building materials and found that wood flooring is a major source of VOC emissions

for formaldehyde, acetaldehyde, cyclohexanone, and benzaldehyde which confirmed the results from Shin and Jo (2012). They also found that the wood flooring and the protective coating on the flooring were both sources of VOCs, which could be the reason the emission rates were much higher than other sources where the wood was not treated with a protective coating.

For indoor air samples, individual VOC concentrations range from a few parts per billion (ppbv) to a few hundred ppbv with a total VOC concentration around 1part per million (ppmv) (Queffeulou et al., 2010; Salonen et al., 2009). Even though these concentrations are very low they can build up to fairly high levels over time because today both homes and commercial buildings are being built to be as air tight as possible in order to be optimize their energy efficiency. This means that the contaminated air is re-circulated over and over again throughout the buildings, which results in a steady increase in contaminant levels. The main concern with VOCs is that they pose serious health problems. At elevated concentrations they can cause eye and skin irritation, and prolonged exposure to low concentrations can cause headaches, nausea, and respiratory problems (Sakamoto et al., 1999). VOCs are also the cause of many unpleasant odors in the air and are responsible for what has been labeled "sick building syndrome". Kabir and Kim (2011) studied the emissions of VOCs from foods during different cooking methods to measure their odor intensities (OI). They found that toluene and acetaldehyde in some cases did exceed the OI ranges recommended by the World Health Organization (WHO). They also found that reduced sulfur compounds had the highest OIs followed by aldehydes and acidic compounds. Salonen et al.,(2009) studied 520 air samples from 176 office buildings to determine if there was a connection between elevated VOC levels and any adverse health effects. In 23 office buildings, elevated levels of formaldehyde were present, and in those 23 buildings reports of upper respiratory tract symptoms (a side effect of exposure to formaldehyde) were more frequent. Because the formaldehyde levels in the air were below the WHO recommended levels, the authors were not able to directly relate the respiratory symptoms with the presence of formaldehyde in the air, but the authors do suggest that it is most likely the prolonged exposure to the low levels of formaldehyde present in the air causing most of the "sick building" symptoms that the office workers are experiencing.

Traditionally, VOCs are removed from the air by adsorption onto activate carbon using charcoal filter, scrubbing the gas using water, or by incineration (Cybulski & Moulijn, 2006; Zhong et al.,

2010). Although these methods have been proven to be effective, they also pose their own problems. Both adsorption and scrubbing require secondary treatment processes to deal with the disposal of the charcoal and contaminated water since the VOCs are only transferred to another medium and not converted into inert chemicals (Lin et al., 2013). For incineration, the air is passed through a furnace where the VOCs are oxidized into various intermediate products before being converted into CO_2 and H_2O. However, in order to obtain complete combustion in the incinerator, it must run at a very high temperature for a sufficient residence time that is very energy intensive and can be expensive. Additionally, the incinerator requires precise temperature control for complete combustion that will vary based on the VOC being treated. If complete combustion is not achieved the produced by-products require further treatment (Cooper & Alley, 2011; Lin et al., 2013). Also, these treatment methods are not designed to operate effectively under the low contaminant concentrations that are present in indoor air since their main applications are for industrial processes, which contain higher VOC concentrations than those found in indoor air. As a result, they cannot easily be employed for home or commercial use.

1.2 Advanced Oxidation Process (Photocatalytic Oxidation)

A new method for treating VOCs in the air is photocatalytic oxidation (PCO). This method uses Ultraviolet (UV) light to activate a catalyst surface that reacts with water and oxygen molecules to produce highly reactive oxidizing radicals. These radicals will then oxidize the VOCs on the surface of the catalyst and convert them to carbon dioxide and water (Hodgson et al., 2007; Pichat, 2010; Zhao & Yang, 2003). The PCO process offers many advantages over traditional treatment methods. First, unlike scrubber columns or charcoal filters, the PCO process is ultimately able to break down the VOCs into carbon dioxide and water. Consequently, it does not require any secondary treatment processes. Second, the process takes place at room temperature and pressure, so it is much more energy efficient than incineration. Third, the titanium dioxide (TiO_2) catalyst that is typically used for PCO systems also has the advantage of being safe to handle, so it will not pose additional health or safety risks. It is chemically inert (will not take part in the oxidation reaction) and will only become activated under UV exposure. TiO_2 is also fairly inexpensive and the processes for coating the support material are very simple. Finally, the TiO_2 catalyst also has a high photocatalytic efficiency and is able to oxidize a large

range of VOCs, which has been shown in multiple studies (Alberici & Jardim, 1997; Destaillats et al., 2012; Hodgson et al., 2007; Obee & Brown, 1995).

1.2.1 Surface Mechanism

During the PCO process the VOCs undergo a series of mass transfer steps: (1) VOCs travel through the bulk air by convection, (2) VOCs diffuse through a water boundary layer to the surface of the catalyst, (3) VOCs adsorb onto the catalyst surface, (4) the VOCs undergo a surface reaction, (5) the reaction products desorb from the catalyst surface, (6) products diffuse back through the boundary layer, (7) products leave the PCO system with the bulk air (convection). The first water boundary layer is formed by water molecules in the air that bond to the catalyst surface (hydrogen bonds). Additional layers of water molecules will form by water molecules bonding together through hydrogen bonds. The thickness of the water boundary layer will depend on the relative humidity (RH) level of the air.

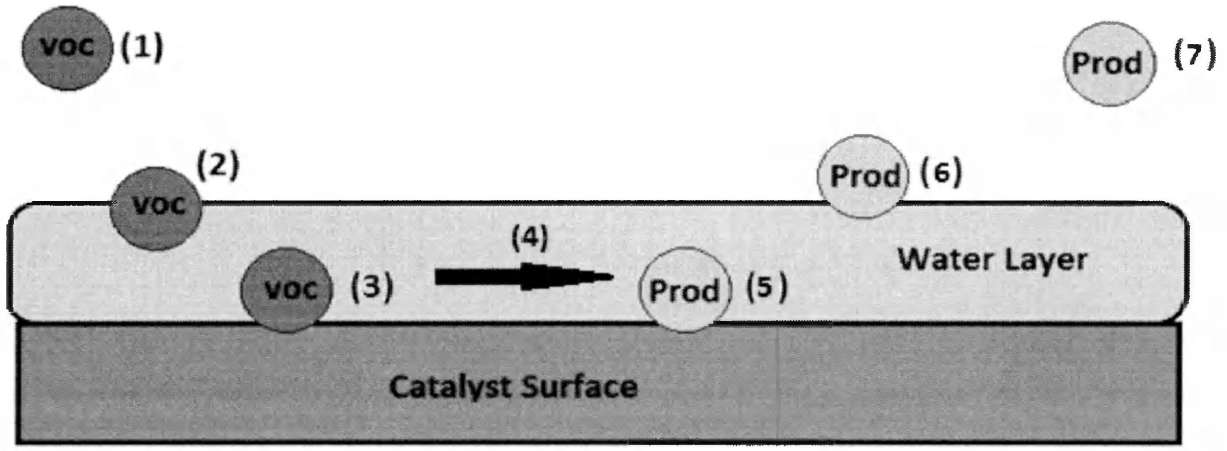

Figure 1: Mass transfer steps of PCO system

When the TiO_2 photocatalyst is irradiated by UV light, valence electrons are excited to the point that they jump from the valence band to the conduction band leaving behind a hole in the valence band.

$$TiO_2 + h_v \rightarrow h^+ + e^- \quad (1)$$

This produces electron (e^-) –hole (h^+) pairs, where the holes (h^+) are now free to react with water molecules on the surface to form the highly reactive hydroxyl radicals,OH^*. The electrons

(e^-) react with oxygen molecules that are present at the catalyst surface to produce superoxide radicals,O_2^-. Both radicals are highly reactive and are able to oxidize a wide range of VOCs(Pichat, 2010).

$$H_2O \rightarrow OH^- + H^+ \quad (2)$$

$$h^+ + OH^- \rightarrow OH^* \quad (3)$$

$$O_2 + e^- \rightarrow O_2^- \quad (4)$$

$$VOC + O_2^- + OH^* \rightarrow CO_2 + H_2O + Other\ Products \quad (5)$$

1.2.2 Catalyst Material

TiO_2 is the most commonly used photocatalyst because it has a very high photoactivity and is very stable (Mo et al., 2009). Mo et al., (2009b) compared the results from 12 different catalyst materials. The authors compared a pure TiO_2 catalyst with TiO_2 catalysts doped with different additives. Overall, the authors found that most additives did not improve the performance of the catalyst. The one exception was silicon dioxide, SiO_2, which did improve the performance of the catalyst slightly by increasing the surface area of the catalyst.

How the catalyst is prepared and coated onto the support material affects the properties of the catalyst particles, most importantly the surface area of the catalyst. Shiraishi et al., (2009) used two thin film methods to coat the same TiO_2 catalyst onto a glass tube. The first method converted amorphous TiO_2 to anatase TiO_2 through calcination at high temperatures, while the second method used slow drying of aqueous anatase TiO_2 dispersion. They found that method one resulted in very smooth surface due to the TiO_2 particles being much smaller than those resulted from the second method. The slow drying at a low temperature resulted in a very rough surface, which gave a much greater reacting surface area. For this reason the rate of formaldehyde decomposition was 53 times higher for method two than for method one. Again, it is shown that the size of the TiO_2 particles plays a large role in the effectiveness of the catalyst by altering the surface area.

There are other factors that should be considered when designing a new system. For example, the fouling on the surface of catalyst over time will be an issue. Some persistent VOCs may not

completely decompose and produce intermediate products. These intermediate products can block the active sites on the catalyst surface, which is referred to fouling of the catalysts. Research has shown that the fouling of the catalyst by intermediates can be reversed by exposing the catalyst surface to air with a high humidity and high UV irradiation (Zhong et al., 2010).

1.2.3 Reactor Configurations

When designing a PCO reactor, the reactor should be able to handle a high volume throughput with a low pressure drop while maintaining sufficient contact between the photons, catalyst, and contaminants in order to oxidize the VOCs. There are 3 main types of reactors that show high VOC removal. Each type has advantages and challenges. First, the honeycomb monolith reactors, which have been studied for use in automobiles for controlling emission exhausts and in power plants for reducing NOx production (Cooper & Alley, 2011; Raupp et al., 2001). In this case, the catalyst is fixed on a monolith. Air passes through the holes and the UV lamps are mounted horizontally in front of the screens. This method has the potential to remove both VOC and particulate matter from the air depending on the support material (Raupp et al., 2001). However, the geometry of the catalyst support also makes it difficult to maintain a constant light intensity across the catalyst and this can cause shadowing on the surface, which will reduce the efficiency of the catalyst. This design could be used for applications in homes or commercial buildings where smaller air filters are already being used within the air systems.

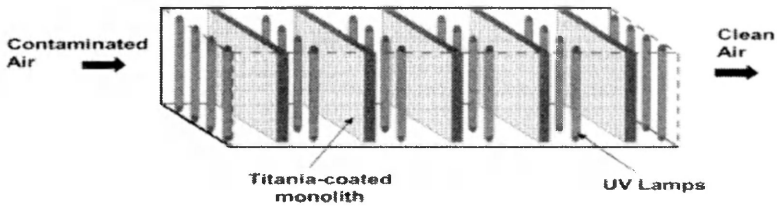

Figure 2: Monolith system (Raupp et al., 2001)

The second is the fluidized-bed reactor which contains packing material (usually glass beads) that is coated with the catalyst (Zhao & Yang, 2003). This design can handle very high gas flow rates while maintaining a low pressure drop and improving contact between the catalyst and the contaminants due to the increased catalyst surface area. The UV lamp may be mounted either in the center or off-center of the reactor. Considering either installation, it can be difficult for the UV light to penetrate deeply into all of the fluid bed evenly (Zhao & Yang, 2003). The

shadowing of UV light within this system reduces the overall performance dramatically. This setup would be best suited for applications where a very high flow rate of air must be treated and where either the VOCs might be corrosive to the monolith support mater or the PCO system cannot be fitted directly into the duct lines of the home or commercial building.

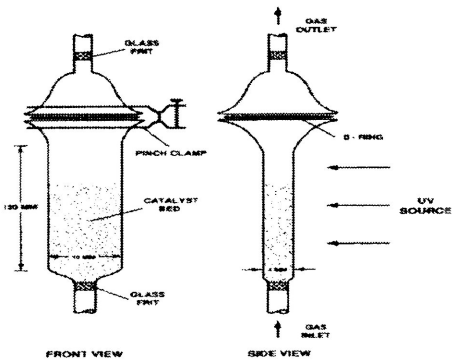

Figure 3: Fluidized-bed reactor (Zhao & Yang, 2003)

Finally, the annular reactors are made up of a glass cylinder with a UV lamp mounted in the center. In this case, the catalyst is coated onto the inside of the glass cylinder. This setup allows for an even light distribution across the catalyst surface and maintains a high flow rate with efficient contact between the catalyst and contaminants (Shie et al., 2008).

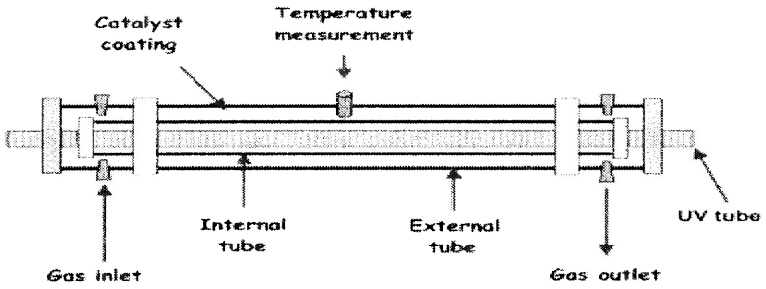

Figure 4: Annular reactor (Keller et al., 2003)

1.3 Reaction Kinetics

In an experimental setup, it is not possible to measure the exact concentration of VOCs on the catalyst surface. So, for this reason, the VOC levels are being measured from the bulk of the system. This means that the rate expressions being derived from experimental data will be a combination of the reaction kinetics, mass transfer effects within the system,

adsorption/desorption of VOCs from the catalyst surface, and diffusion effects of the VOCs through the boundary layer.

1.3.1 Kinetic Models

With indoor air VOC concentrations in the range of several ppbv to a few hundred ppbv, the reaction kinetics are going to be different that those determined for higher VOC concentrations, which have been tested in the labs (in the range of tens of hundreds of ppmv). All PCO studies have found that the reaction rate of VOCs at the catalyst surface does not follow simple first order kinetics, but they tend to follow some variation of the Langmuir-Hinshelwood (L-H) kinetic model where the kinetic rate constants, k', is a combination of both the reaction rate constant, k, and the adsorption rate constant, K_{ads} (Alberici & Jardim, 1997; Assadi et al., 2012; Brosillon et al., 2008; Deveau, et al., 2007; Lopes, et al., 2012).

$$r = k' \frac{K_{ads} C_{VOC}}{1 + K_{ads} C_{VOC}} \tag{6}$$

Where r is the reaction rate

k' is the kinetic rate constant

K_{ads} is the adsorption rate constant

and C_{VOC} is the target VOC concentration in the system

The L-H kinetic model can describe most phenomena happening on the surface of the catalyst, such as adsorption, surface reaction, and desorption. As a result, the L-H correlation is the most appropriate kinetic model to describe the kinetics of PCO reactions. Experimentally, it is not possible to accurately monitor what is happening at the catalyst surface. So, when developing the L-H kinetic models it is common practice to use the bulk concentration for the target VOC to describe the rate of reaction happening at the catalyst surface. Alberici and Jardim (1997) studied the degradation of 17 different VOCs using a PCO system and found that all 17 of the VOCs followed an L-H kinetic model. The 17 VOCs covered a wide range of organics that included alkanes, aromatics, chlorinated compounds, acetyls, alcohols, ketones, and ethers. This study, along with numerous studies on individual VOCs covers the wide range of VOCs found in

indoor air and shows that the L-H kinetic model can be used to describe the decomposition of all VOCs during the PCO process.

1.3.2 Effects of Operating Parameters

There have been many experimental studies on PCO treatment of VOCs in air, which have looked at the effects of temperature (Obee & Brown, 1995; Shiraishi et al., 2005a; Zhong et al., 2010), relative humidity (RH) (Pichat, 2010; Zhao & Yang, 2003), flow rate (Lee, et al., 2012; Shiraishi et al., 2005b), VOC concentration (Brosillon et al., 2008; Hodgson et al., 2007), and UV light intensity (Brosillon et al., 2008; Queffeulou et al., 2010; Shie et al., 2008) on the degradation rates of various VOCs.

1.3.2.1 Temperature

When evaluating the effects of temperature on a PCO process, there are two phenomena that must be considered. First, the rate of reaction is related to temperature by the Arrhenius equation. As a result, the rate of reaction increases as the temperature of the catalyst is increased. The second factor that must be considered is the effect of temperature on the rate of adsorption/desorption, of the VOC onto the catalyst surface. When the surface temperature is increased there is a drop in the rate of adsorption/desorption, which was observed by Zhong et al., (2010) and Obee and Brown (1995). It can be concluded that there is an optimal temperature range for each PCO system where a balance between reaction kinetics and adsorption effects is achieved. Shiraishi et al.,(2005a) looked at the effects of air temperature on the rate of formaldehyde decomposition for air temperatures between 45°C and 90°C. They found that as they increased the air temperature beyond 45°C the removal efficiency decreased. The same trend was also recorded by Obee and Brown (1995). It may be concluded that PCO reactions do not favor high temperatures and the process should be carried out at room temperature. It also may imply that temperature has a greater effect on adsorption/desorption effects rather than the reaction kinetics.

1.3.2.2 Relative Humidity (RH)

Similar to temperature, when evaluating the role of RH two effects must be considered since the water molecules in the air play two different roles in the oxidation process. First, they act as a source for OH radicals that will oxidize the VOCs in the air. It is expected that the rate of

reaction will increase with increasing relative humidity since this would allow for more oxidizing radicals to be produced at the catalyst surface. On the other hand, an increase in the RH will also cause an increase in the boundary layer thickness which would hinder the mass transfer of the VOCs to the catalyst surface. An excess of water vapor on the catalyst surface will reduce the amount of active sites available for the organics and decrease the rate of adsorption, which in turn reduces the effectiveness of the catalyst. Again, there is an optimal RH that provides a balance between producing sufficient oxidizing radicals and minimizing the mass transfer effects due to the boundary layer thickness. Assadi et al., (2012) found this balance when studying the decomposition of isovaleraldehyde and trimethylamine. For both contaminants initially there was an increase in the rate of decomposition as more oxidizing radicals were being produced. This was followed by a drop in the rate of decomposition as the mass transfer effects began to dominate the reaction. For isovaleraldehyde the optimal range was 35-45% RH and for trimethylamine a range of 20-30% RH was optimal. For indoor environments, it is recommended that a RH between 30% and 60% be maintained (Canadian Lung Association, 2012). So, it can be seen that for most VOCs the optimal RH range will be within the recommended indoor air levels. This means that no additional humidification or dehumidification should be required.

1.3.2.3 Flow Rate

The flow rate of the air will impact the mass transfer of the VOCs. In order to maintain sufficient contact between the catalyst and the VOCs, the flow rate must be large enough to ensure that the reaction is not mass transfer limited (turbulent vs. laminar mass transfer). As the velocity is increased the residence time of the VOCs is shortened, which reduces the chance that the VOCs will make contact with the surface of the catalyst. Determining the optimal flow rate for the chosen reactor configuration is important in order to avoid mass transfer limitations on the decomposition of the VOCs. This factor is even more pronounced at low air velocities (laminar flow conditions) where the flowing air can produce a second boundary layer on top of the water layer. These effects were seen by Charles et al., (2011) and Lopes et al., (2012) where the low flow rates resulted in additional mass transfer effects within their systems. Lee et al., (2012) also observed both of these effects when they determined removal efficiency of dimethyl sulfur (DMS) by changing the flow rate of the air and the residence time in the reactor. They

used different reactor inlets to alter the stream length of the contaminated air so that they could evaluate the effects of both linear velocity and residence time to optimize the PCO reactor design. As the residence time was increased, increasing the length of the streamline, the system was able to achieve a higher conversion of the target VOC for the same linear velocity. The authors also found that for all of the four reactor setups they all reached an optimal linear velocity around 0.255 m/s which gave a balance between minimizing mass transfer effects and providing sufficient residence time.

1.3.2.4 VOC concentrations and Mixture

Overall, it is expected that the rate of VOC decomposition is increased as the initial VOC concentration is increased since the rate of reaction is directly related to the VOC concentration. The typical VOC concentrations in indoor air are in the ppbv range. At such low levels, an increase in the initial VOC concentration will increase their chance of adsorbing onto the catalyst surface. This trend is consistent with other studies, which looked at individual VOCs (Brosillon et al., 2008; Charles et al., 2011; Lopes et al., 2012; Ohko et al., 1998). A large number of PCO studies focused on decomposition of one or two VOCs in the air, but in reality there could be hundreds of VOCs present in an indoor air sample. When more than one VOC presents, the individual VOCs must compete with one another, along with water and oxygen molecules, for the active sites on the catalyst surface. There are a few studies of PCO processes using mixtures of VOCs in air (Alberici & Jardim, 1997; Assadi et al., 2012; Hodgson et al., 2007) and it would appear that the rate of oxidation is proportional to the size of the molecules. Larger VOCs tend to have higher oxidation rates than VOCs with smaller molecular weights. This could be due to the fact that larger VOCs will break down to smaller VOCs before being completely decomposed to CO_2 and H_2O. However, this was only seen when VOCs were present at levels higher than the ppbv range found in indoor air. Assadi et al., (2012) performed the same set of experiments for the decomposition of isovaleraldehyde and trimethylamine (both complex VOCs) and found that there were measurable levels of by-products produced when the initial VOC concentrations were in the ppmv range. When the initial VOC levels were decreased to the ppbv range there were no detectable levels of byproducts found which would imply that the VOCs were being completely mineralized at the lower levels. This would imply that when VOCs are present in the ppbv range the VOCs are completely decomposed on the catalyst surface and no intermediate products are

produced. Hodgson et al., (2007) studied the decomposition a complex VOC mixture made up of 27 VOCs found in office and building and cleaning solvents. They found that not all VOCs will react simultaneously and the larger or more complex VOCs tend to decompose first, followed by the smaller and less complex VOCs. Overall the order of oxidation was as follows: alcohols, glycol ethers > aldehydes, ketones, terpenes > aromatics, alkanes > halogenated aliphatic hydrocarbons.

1.3.2.5 UV Source and Intensities

The light intensity, or photon flux, emitted from the UV lamp determines the activity of the catalyst surface. When the light intensity[1] (I) is around 1-2 mW/cm^2 at the catalyst surface the rate of oxidation will increase with the light intensity by a factor of$I^{0.5}$. When light intensity drops below 1 mW/cm^2 the rate of oxidation will increase linearly with the intensity (Obee & Brown, 1995). In order to activate the surface, UV lamps with wavelengths between 300 and 365 nm are required, which can be done using both UVA and UVC lamps and even UV-LED lamps have been explored. Shie et al., (2008) studied the decomposition of VOCs under UVA, UVC, and UV-LED light sources and found that all three have similar removal efficiencies and were effective UV sources. They did note that the UVLED system was much more energy efficient than the UVA or UVC sources. These results were consistent with other studies on the use of different light sources (Alberici & Jardim, 1997; Destaillats, et al., 2012). Although all three light sources have been found effective for PCO processes, UV-A and UV-C lamps are the best option since they are a much more cost effective option than UV-LEDs which are very expensive. Additionally, many UV-LEDs would be required to cover the same area as one UV-A or UV-C lamp covers. If UVC lamps are being used extra precautions should be taken to ensure that all UVC light is contained within the PCO system to eliminate any human contact.

1.4 Summary of Experimental Work

There are many advantages of using photocatalytic oxidation for VOC removal. This process does not require any secondary treatment since the organics are completely broken down into CO_2 and H_2O. It also does not require any additional oxidizing agents to be added to the process since the water and oxygen molecules in the air are easily converted into strong oxidizing agents on their own. The TiO_2 catalyst is also fairly inexpensive and is very stable and safe to handle. It is also a very efficient photo catalyst and can operate at room temperature and pressure. There

are a few facts that must be considered using a PCO system. First, the catalyst can become deactivated after a period of time. It will either need to undergo a reactivation process or it will have to be replaced. Second, reaction residue can be generated by intermediate products which occupy active sites, or particulate matter in the air can block the pores and cause fouling of the catalyst surface. Although a method to regenerate the catalyst has been proposed it has not yet been found to be efficient or cost effective (Zhong et al., 2010). Third, the UV lamps will experience fluctuations in their light intensities at the beginning and the end of their life spans. These variations can have significant impacts on the activity of the photo catalyst which will alter the rate of decomposition of the organics.

There are several issues faced by laboratory studies of VOC removal. The very low concentrations of contaminants can make it difficult to accurately measure the contaminant levels in the effluent. It is also not possible to study the effect of multiple operating parameters at once without knowing their interactions with each other. In a lab setting it is also not possible to efficiently monitor the profile of contaminant concentration over the length of the reactor. As a result, just the overall effects are reported.

Overall a PCO system appears to be a very feasible and cost effective method for treating VOCs in the air in an indoor environment for very low concentration of contaminants. The PCO process seems to be optimized around ambient conditions (temperature and relative humidity), inexpensive materials (TiO_2 catalyst, UVA or UVC lamps), and the reactor setup is a fairly simple design (monolith or annular reactor). Both reactor setups could also easily be retrofitted into an existing air system within a home or office building, which again lends to the PCO process being a cost effective option.

1.5 Computation Fluid Dynamic Modeling

Fluid processes can be simulated using Computational Fluid Dynamics (CFD) by simultaneously solving different transport equations. For PCO processes, three sets of transport equations must be solved: hydrodynamics, radiation, and species transport. CFD models can provide a better understanding of how reacting species behave throughout the different parts of the system because the concentration of contaminants can be monitored through the system under different operating conditions. In a lab setting, it is only possible to study overall reaction kinetics, measuring the concentration of the contaminants at the inlet and outlet. Practically, it is not

possible to measure the concentration profile along the reactor or on a specific surface with no interferences. Being able to better understand the interactions between competing parameters will allow us to optimize the reactor design for VOC removal for a variety of operating conditions and applications (Huang et al., 2011). CFD modeling can also be more cost effective because it does not require different reactor setups to determine the most efficient geometry. The bulk section of the reactor can be modified to optimize the hydrodynamics of the system without altering the catalyst structure (or the rate of reaction at the catalyst surface). For these reasons CFD is quickly becoming a key factor in the design and optimization of PCO systems and other engineering applications (Duran et al., 2010; Wang et al., 2012).

1.5.1 Hydrodynamic modeling

The first model that must be solved is the hydrodynamic model, which has been well developed for both laminar and turbulent flow conditions, based on the Navier-Stokes equation. In order to solve the hydrodynamic model two conservation equations are solved simultaneously:

$$\text{Conservation of mass:} \quad \frac{\partial \rho}{\partial t} + \nabla(\rho v) = 0 \tag{7}$$

$$\text{Conservation of momentum:} \quad \frac{\partial \rho v}{\partial t} + \nabla \rho v v = -\nabla \rho + \nabla \tau + \rho g + S_m \tag{8}$$

Where ρ is the density of the air

t is time

v is the velocity

and τ is the stress tensor.

1.5.2 Radiation field modeling

Using CFD, the radiation field can be calculated on throughout the reactor and on the surface of catalyst using the radiative transport equation:

$$\frac{dI(r,s)}{ds} + (a + \sigma_s) I(r,s) = an^2 \frac{\sigma T^4}{\pi} + \frac{\sigma_s}{4\pi} \int_0^{4\pi} I(r,s) \Phi(s,s)\, d\Omega' \tag{9}$$

where r is the position vector

s is the direction vector

a is the absorption coefficient

$\sigma_s$is the scattering coefficient

n is the refractive index

T is the temperature of the air

and Ω' is the solid angle.

The uniformity of the radiation field depends on the strength of the irradiance at the surface of the catalyst and the geometry of the reactor. In PCO studies, it is common practice to assume that a uniform intensity is being produced across the entire catalyst surface. However, this assumption is not generally the case as the radiation field will vary along the length of the reactor and along the length of the UV lamp itself.

1.5.3 Species Transport

The changes in species concentrations due to convection, diffusion, and the surface reaction are modeled by the species transport equation, which must be solved for each of the reacting species:

$$\frac{\partial}{\partial t}(\rho Y_i) + \nabla \cdot (\rho v Y_i) = -\nabla \cdot J_i + S_i \tag{10}$$

Where Y_i is the mass fraction of species i

ρ is the density of the air

S_i is source or sink term of species i

and J_i is the effective flux of species i.

1.6 PCO Modeling Work

Compared to the number of experimental studies, CFD studies for PCO air systems are very limited. Individual studies focused on validating the individual model components for hydrodynamics have been conducted (Kumar & Bansal, 2012; Zhang et al., 2012), UV radiation (Imoberdork et al., 2008), and species transport (Liu & Peng, 2005; Queffeulou et al., 2010a) but only a handful of studies have tried to combine all three models into a single study (Chong et al., 2011; Hossain et al., 1999; Wang et al., 2012).

Kumar & Bansal (2012) performed an in depth CFD study in order to validate the use of CFD modeling to predict hydrodynamics and species distribution within an annular reactor. The

authors looked at three parameters to compare the CFD predictions against theoretical and empirical formulas: velocity distribution, average velocity, and average mass transfer coefficient. They looked at the case of laminar flow conditions for water containing Rhodamine B, an organic dye. Using the conservation of mass, momentum, and species equations, the authors were able to match the expected trends for laminar flow conditions. They found that all three parameters estimated using CFD were within 2.1 - 10% of the theoretical values for fully developed laminar flow.

Wang et al., (2012) used CFD to model the radiation field of a UV LED array system for a UVLED PCO reactor. The LED array system contained 27 UV LEDs arranged in a 3x9 array structure. The authors developed their own radiation model in order to describe the irradiance distribution on the catalyst surface. Their model calculated the relative irradiance distribution on the catalyst surface in terms of position relative to the LED. Assuming each LED lamp has identical properties, the incident irradiance at a particular point on the catalyst surface was determined to be the sum of the values from each of the 27 LED. Using their radiation model they were able to map the irradiance levels within the system and compared the results with levels that were measured experimentally. The CFD model predictions were in agreements with the experimental values. The authors were also able to optimize the system by changing the distance between the lamp array and the catalyst surface in order to obtain a uniform irradiance field across the catalyst surface.

1.7 Scope of Research

The focus of this research was to develop a new approach to modeling surface reactions for the treatment of air using the PCO process. An integrated CFD model was developed to consider hydrodynamics, species transport, including reaction kinetics, and radiation based on experimental PCO systems. In order to validate the CFD work, published data was used to build the CFD model of a PCO process and the final CFD results were compared to those that were published previously. An integrated model provides the opportunity to fully understand the interactions between different operating conditions and to see how the contaminants are moving through the reactor, which would not be possible to see in the lab.

The work described in this thesis was completed in three stages. The first stage involved developing a new approach to modeling complex surface reactions for a PCO reactor system.

This new approach allowed for the experimental reaction rates and a combination of both reaction kinetics and mass transfer effects, to be adapted in order to describe only the reaction kinetics on the surface of catalyst. In this first case, the work of Shiraishi et al., (2005b) was modeled where formaldehyde is decomposed using an annular PCO reactor in a closed system. Three different approaches to defining the reaction rate model were tested. Since Shiraishi et al., (2005a) did not consider changing UV intensities on the catalyst surface, this first case does not require solving the radiation model. The complete CFD model required solving the hydrodynamic model and the species transport models. In this case the reaction rate model was a function of formaldehyde concentration at the catalyst surface. The final model results were then compared with the published results by Shiraishi et al., (2005b) in order to validate the integrated CFD model, excluding the radiation model.

The second stage of this work involved using the new approach for reaction modeling of a complex PCO system that was developed in the first stage. In the second stage, the work of Brosillon et al., (2008) was modeled where air contaminated with butyric acid was treated using a coaxial monolith PCO reactor. In this case the rate of reaction was a function of both the butyric acid concentration and the UV light intensity at the catalyst surface. The reactor setup was also more complex and contained two reacting surfaces. The CFD model in this case required solving the hydrodynamic, radiation, and species transport models. Once the complete model was obtained, the results were compared with those published by Brosillon et al., (2008) to validate the model results. From this case, the versatility of this new approach to reactor modeling was demonstrated.

In the final stage of the work, the new protocol was used to demonstrate the potential applications of this research. Butyric acid is a carboxylic acid that is naturally secreted by the human body so using the results from the second stage of this work; a CFD model was developed to virtually study a PCO system within the air duct system of a closed room. The PCO system was tasked with treating air already contaminated with butyric acid as well as being exposed to a point source for butyric acid present within the closed room. The point source represented a person in the room that is giving off butyric acid. The final part of this thesis discusses other potential applications of this research.

Chapter 2 – Developing a New Method of Reaction Modeling

2.1 Introduction

Considering the experimental research performed for photocatalytic reactions, for continuous open systems (no air recirculation) samples of the air are taken at the entrance and the outlet of the system. For closed systems, the samples of air are taken before turning on the UV lamps and then periodically from the bulk of the system. As a result, the reaction rate expressions provided by the experimental work are volumetric reaction rates in terms of the total reactor volume. In these cases, the VOC concentrations will be an average across the entire system, which results in the reaction rates being a combination of reaction kinetics and mass transfer effects. This gives an overall apparent photochemical kinetic rate expression that may be lower than the actual rate of reaction at the catalyst surface. Particularly for a laminar system, the overall reaction rate expression will be much lower than the actual rate of reaction happening on the catalyst surface since the concentration of VOCs in the bulk of the system is higher than the concentration of VOCs at the catalyst surface. For this reason the experimental reaction rates cannot be used directly to define the rate of reaction at the catalyst surface. The species conservation equation takes into account velocity profile (convection term for mass transfer) and molecular diffusion within the system. As a result, the reaction rate model must reflect the actual rate of reaction at the catalyst surface. This chapter introduces the new approach to modeling complex surface reactions, which uses the volumetric experimental data to define a surface reaction.

2.2 Theory

2.2.1 A Novel Approach to Defining Reaction Rate Model

The CFD software (Ansys Fluent version 14.0) used for this research project does have built in reaction models; however, these models are not capable of modeling the complex surface reaction rates of PCO systems. For this reason, a novel approach was developed to accommodate the complex surface reactions. This new approach focuses solely on the surface reaction, including absorption and desorption on/from the catalyst surface. As a result, the mass transfer effects within the bulk of the system are separated from the reaction rate expression.

Considering the species conservation equation (Equation 10), it can be noted that the source term, S_i, describes the net addition (or removal) of a species from the system. It should be noted that this term is volumetric base. This can be equated to the production (or consumption) of a species due to a chemical reaction.

$$\frac{\partial}{\partial t}(\rho Y_i) + \nabla \cdot (\rho v Y_i) = -\nabla \cdot J_i + S_i \tag{10}$$

where Y_i is the mass fraction of species i

ρ is the density of the air

S_i is source or sink term of species i

and J_i is the diffusional flux of species i

In a PCO system, the reaction actually takes place in a single layer along the surface of the catalyst material just below the water boundary layer. Computationally, this cannot be implemented in the CFD model because the infinitesimally small thickness of the layer (a few angstroms) cannot be modeled from a practical standpoint. So, the source term is considered as the reaction rate term along a very small single layer of cells adjacent to the surface of the catalyst and with the units of kg/m^3-s. In other words, a thin layer above catalyst surface behaves as a volumetric reactor. As a result, Equation 10 is used to model the concentration of species on the surface of the reactor. The source term is zero for the other locations.

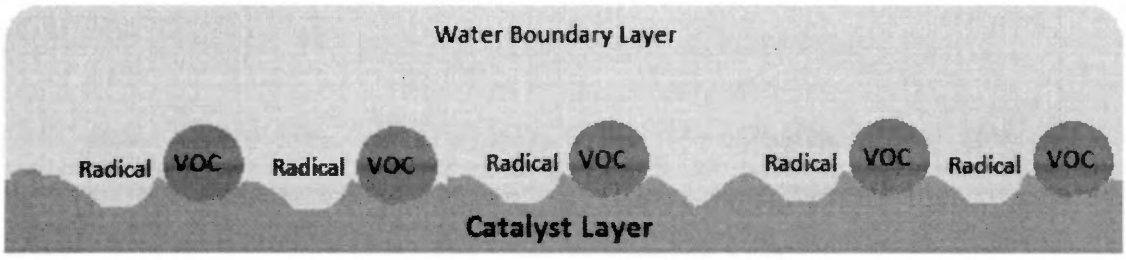

Figure 5: Surface Reaction Diagram

It has been shown through the extensive experimental work that PCO reactions follow the L-H kinetic model, which was described in Chapter 1. The rate expressions are derived using the average concentration of the target VOC from the bulk of the system. These concentrations

reflect the concentration of the VOC across the entire system volume, which results in an overall volumetric reaction rate expression:

$$rate_{volumetric} = k' \frac{K_{ads} C_{voc}}{1 + K_{ads} C_{voc}} \quad (11)$$

Considering the experimental data, it is assumed that the reaction is taking place across the entire system volume giving a rate of reacting per unit volume of the entire system. For a surface reaction, a similar assumption can be made that the reaction is taking place across the entire reactive surface, giving a rate of reaction on a per unit surface area basis. So, in order to adjust the experimental volumetric reaction rate expression so it can be used as the surface reaction in terms of total reactive surface area, the following correlation is derived:

$$rate_{surafce} = rate_{volumertic} \left(\frac{V_{system}}{SA_{catalyst}} \right) \quad (12)$$

Where $rate_{surface}$ is the rate of reaction in terms of catalyst surface area

$rate_{volertic}$ is the rate of reaction in terms of system volume

$SA_{catalyst}$ is the total catalyst surface area

and V_{system} is the total system volume

Numerically solving the conservation equations, the system is divided into a finite number of elements (cells). Using Equation 12, the rate of reaction per unit of total catalyst surface area can also be used to define the rate of reaction in terms of the surface area of each cell. The rate of reaction on the catalyst surface is then transformed into a volumetric rate of reaction in terms of the individual cell volume for the entire layer of cells adjacent to the catalyst surface by the ratio of cell volume to the cell surface area:

$$rate_{cell\ volume} = rate_{surface} \left(\frac{SA_{cell}}{V_{cell}} \right) \quad (13)$$

With the reacting volume being the layer of cells just above the catalyst surface, the rate of reaction will now be dependent on the concentration of the VOC within that volume, which will be the same as the concentration of the VOC on the catalyst surface.

The reaction rate model is then introduced into the CFD model along the catalyst surface as the S_i term in the species transport model for each of the reacting species. The reaction rate model is developed in terms of the complete decomposition of the target VOC. For the other reacting species, the rate of decomposition or production will be adjusted using stoichiometric ratios (a, b, c, or d) for complete decomposition.

$$aVOC + bO_2 \rightarrow cCO_2 + dH_2O \tag{14}$$

2.2.2 Hydrodynamic Model

The flow of air through the system is modeled by solving the conservation of mass and the conservation of momentum equations, which have been well developed for both laminar and turbulent flow conditions based on the Navier-Stokes equation. In order to solve the hydrodynamic model, the two conservation equations should be solved simultaneously:

$$\text{Conservation of mass:} \qquad \frac{d\rho}{dt} + \nabla(\rho v) = 0 \tag{15}$$

$$\text{Conservation of momentum:} \qquad \frac{\partial \rho v}{\partial t} + \nabla \rho v v = -\nabla \rho + \nabla \tau + \rho g + S_m \tag{16}$$

Where ρ is the density of the air

t is time

v is the velocity vector

τ is the stress tensor

g is the gravitational constant

and S_m is the momentum source term

Under laminar flow conditions, the velocity profile is uniform with the fluid traveling in a linear direction, Figure 6. This can result in a secondary boundary layer being produced by the air along the catalyst surface, which creates an additional mass transfer barrier for the reaction to overcome. This is not ideal for reacting systems with surface reactions. Under turbulent flow conditions, the air moves in a disorganized manner that results in mixing of the air along the reacting surface, which helps to improve the mass transfer effects at the surface.

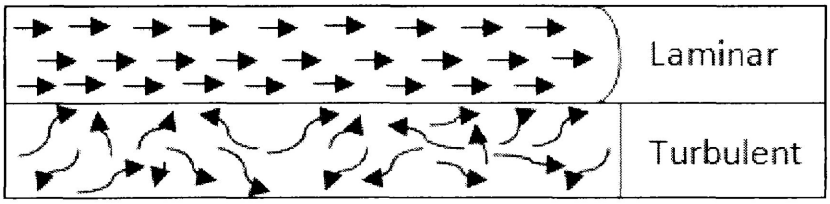

Figure 6: Flow profile comparison

2.2.3 Turbulence Model (k-epsilon)

For turbulent flow conditions, there is no linear flow profile, so a time average velocity across each cell must be estimated. The most common approach to solving this is by using the Reynold-averaged form of the conservation equations, which generates new variables as Reynold stresses or turbulent stresses. To solve the new unknowns, two more conservation equations are introduced. The most common model used is the standard $k-\epsilon$ model due to its simplicity along with its accuracy across a wide range of turbulent flow conditions (Launder & Spalding, 1974). The standard $k-\epsilon$ model solves for the turbulence kinetic energy,k, and the dissipation rate, ϵ, using the following two equations:

$$\frac{\partial}{\partial t}(pk)+\frac{\partial}{\partial x_i}(pku_i)=\frac{\partial}{\partial x_j}\left[\left(\mu+\frac{\mu_t}{\sigma_k}\right)\frac{\partial k}{\partial x_j}\right]+G_k+G_b-p\varepsilon-Y_M \tag{17}$$

$$\frac{\partial}{\partial t}(p\varepsilon)+\frac{\partial}{\partial x_i}(p\varepsilon u_i)=\frac{\partial}{\partial x_j}\left[\left(\mu+\frac{\mu_t}{\sigma_\varepsilon}\right)\frac{\partial \varepsilon}{\partial x_j}\right]+C_{1\varepsilon}\frac{\varepsilon}{k}G_k+C_{3\varepsilon}G_b-C_{2\varepsilon}p\frac{\varepsilon^2}{k} \tag{18}$$

Where $\mu_t$is the turbulent viscosity

Y_M is the effect of compressibility

σ_k and σ_ε are the turbulent Prandtl numbers for k and ϵ

G_k is the generation of turbulence kinetic energy due to the mean velocity gradient

G_b is the generation of turbulence kinetic energy due to the buoyancy respectively

and $C_{1\varepsilon}$, $C_{3\varepsilon}$, and $C_{2\varepsilon}$ are constants which have predetermined values already set within the standard $k-\epsilon$ model, Table 1

The constant values have been rigorously tested using the standard $k-\epsilon$ model and have been found to work for a wide variety of flows.

Table 1: Values of constants for the k-epsilon model

$C_{1\varepsilon}$	1.44
$C_{3\varepsilon}$	1.92
$C_{2\varepsilon}$	0.09

In the case of turbulent flow, the diffusional flux term, J_i, from the species conservation equation will be affected. For laminar flow conditions, the diffusion of the species is controlled solely by molecular diffusion. For turbulent flow conditions, the species experience a second form of diffusion, turbulent diffusion. The effect of the diffusion due to turbulence is determined by the turbulent Schmidt number, Sc_t:

$$Sc_t = \frac{\mu_t}{\rho D_t} \tag{19}$$

Where Sc_t is the turbulent Schmidt number

D_t is the diffusion coefficient due to turbulence

For turbulent flow conditions the diffusional flux term is defined using the following equation:

$$J_i = -\left(\rho D_{i,m} + \frac{\mu_t}{Sc_t}\right)\nabla Y_i - D_{T,i}\frac{\nabla T}{T} \tag{20}$$

Where $\frac{\mu_t}{Sc_t}$ accounts for the effects of diffusion due to turbulence

2.3 First Case Study

2.3.1 Geometry Model and Mesh Structure

Considering the first case, the reactor configuration was based on the closed system set up used by Shiraishi et al., (2005b). Their system used an array of 9 identical reactors placed in a closed box with a total system volume of 1 m^3 under standard room conditions (25°C and 1 atm). Each reactor was comprised of a TiO_2 coated glass tube (28 mm in diameter and 210 mm long) with a UV lamp (15 mm in diameter, 295 mm in length) mounted in the center of each glass tube. All 9 reactors were identical with the same physical and photocatalytic properties. Therefore, only one reactor was modeled with the system volume reduced to 1/9 of the total system volume reported. The reactor also had two symmetric planes and was further divided radially into 4 quadrants. As

a result, only one quarter of a single reactor was modeled. This strategy reduced the computational time dramatically.

Figure 7 shows the cross section of one of the symmetric planes of the reactor model used for the CFD simulation. The reactor section was surrounded by a second glass cylinder (diameter 41 cm), which gave a total system volume of 0.111 m^3. The model of the reactor is identical to the reactor used by Shiraishi et al.,(2005b) with the same ratio of catalyst surface area to system volume (0.167 m^2/m^3). A virtual fan was placed at the entrance to the reactor in order to produce the axial flow through the system, which is similar to the flow rate used in the experiments (Shiraishi et al., 2005b). Once the geometry model was obtained, the mesh structure was established. After using several different mesh densities, the solution reached mesh independent results (the results did not change when the number of cells were increased) for a total number of 32 623 cells.

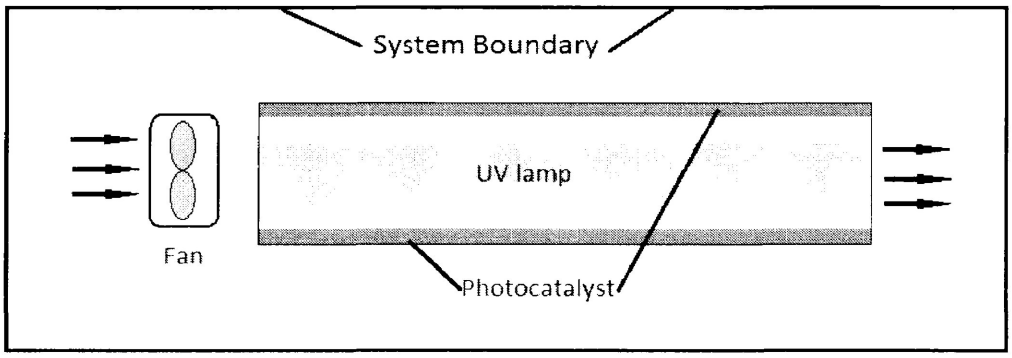

Figure 7: Reactor setup for first case study

2.3.2 Operating and Boundary Conditions

For this study, Ansys Fluent 14.0 was used to model the PCO reactor array developed by Shiraishi et al., (2005b). The $k-\epsilon$ model was selected for modeling turbulent flow. In addition, the species transport equations (one for each reacting species) were modeled simultaneously with the momentum equation. Considering the effect of turbulence on the species mass conservation equation, the default turbulent Schmidt number of 0.7 was initially selected (the Fluent manual states that the default Sc_t value of 0.7 is sufficient for most turbulent systems). The rate of reaction on the surface of the catalyst was developed (see Theory section) using external codes (macros) and integrated into the mass conservation equations for all

reacting species. The reaction rate expressions were implemented into the CFD model as source terms (S_i from Equation 10) using user defined functions (UDFs).

The interior boundary of the fan was set as "FAN". The pressure drop was adjusted to 175 Pa across the fan in order to give the required flow rate of 11.38 m/s (velocity used by Shiraishi et al., (2005b)). The fan direction was selected to pull the air through the reactor section and match the flow direction used in the laboratory experiments.

The simulation was performed for unsteady state condition. Considering the initial conditions, the concentrations of each species were set to match those used by Shiraishi et al., (2005b) and were set as constant concentrations in the bulk of the system: CH_2O 1.23 mg/m^3, O_2 0.205 kg/kg, CO_2 340 ppmv and H_2O RH 30 %. The multicomponent mass diffusivity was selected and the values for each of the species combinations were calculated using standard equations for molecular diffusion for a gas - gas system (Treybal, 1980).

2.3.3 Solution Setup

The SIMPLE discretization scheme was selected using the pressure based solver. The default discretization methods were used for solving all conservation equations. A solution residual of 10^{-4} was selected for all equations except the energy equation, which had a solution residual of 10^{-6}.

In order to establish the velocity profile and initial species distribution, the model was first ran under steady- state conditions with the source term in the species mass conservation equation set to zero. Once the velocity profile was established, the system was switched from steady-state to transient and the source terms in the species transport equation was switched on for all chemical species.

Since the concentration of CH_2O was so low, it was assumed that the density and viscosity of the air were not changing significantly over time. As a result, the velocity profile was not changed, then, the conservation equation for momentum was not solved any more in order to reduce the computation time. A time step of 1 s was chosen, requiring a total of 10,800 time steps to model the 3 hour reaction time used by Shiraishi et al.,(2005b). The time step of 1 s was determined through trial and error over a 30 minute reaction time. For larger time steps (5 s, 30 s and 60 s) the results were not consistent and the model results changed as the time step was altered. For

time steps smaller than 1 s there was no significant improvement in the model results. Therefore, in order to minimize the number of time steps required, a time step of 1 s was ultimately selected.

2.3.4 Reaction Rate Model

Defining the kinetic model, three different approaches were tested and compared with experimental results obtained by Shiraishi et al., (2005b). For each kinetic model the concentration of CH_2O was estimated using an integrated CFD model.

2.3.4.1 First Approach

The first approach used the reaction rate mode proposed by Shiraishi et al., (2005b) using the bulk formaldehyde concentration:

$$r_1 = 0.00093 C_b \tag{21}$$

Where r_1 is the rate of reaction

and C_b is the concentration of formaldehyde in the bulk of the system.

It should be noted that the rate constant suggested by Shirashi et al.,(2005b) had time units of min^{-1} so the rate constant was adjusted to give the time unit of s^{-1} that was required by Ansys Fluent 14.0.

2.3.4.2 Second Approach

The second approach was an exponential model derived from the experimental results of Shiraishi et al., (2005b). For the purpose of reactor design, a closed system can be considered as a batch reactor. For batch processes where the VOCs have low initial concentrations (ppbv) the reaction rate should follow apparent first order kinetics with the reaction rate kinetic constant of the PCO reactor following the L-H kinetic model:

$$r_2 = k_{app} C_b \tag{22}$$

$$k_{app} = \frac{k_1}{1 + k_1/k_2} \tag{23}$$

Where r_2 is the rate of reaction

k_{app} is the apparent first order reaction rate kinetic constant

k_1 is the adsorption/desorption kinetic constant

and k_2 is the surface reaction kinetic constant

At low concentrations the drop in concentration over time can usually be described by an exponential expression in the form of:

$$C_b = ae^t \tag{24}$$

Where a is a constant

and t is the time elapsed

After fitting the experimental data into Equation 22, the rate of formaldehyde decomposition becomes:

$$r_2 = 0.001995C_b \tag{25}$$

2.3.4.3 Third Approach

Finally, the third kinetic model was a two part polynomial reaction rate. A polynomial rate expression was obtained by plotting the change in formaldehyde concentration (in the bulk of the system) over time (dC/dt) versus concentration of CH_2O. The initial rate of formaldehyde decomposition was much higher than the rate of decomposition after 30 minutes. When one polynomial function was applied to the whole data set, the trend did not fit the data very well, in particular at lower CH2O concentrations. In order to match the experimental results, a two part polynomial rate was used in order to obtain more accurate results.

Equations 26 and 27 represent the decomposition rate of formaldehyde when the concentration is above and below 0.76 mg/m3 (or $7.65\text{x}10^{-7}$ kg/kg), respectively.

$$r_{3a} = -779C_b^2 + 0.00187C_b - 7.05\text{x}10^{-10} \tag{26}$$

$$r_{3b} = -2.56\text{x}10^{22}C_b^5 + 5.5\text{x}10^{16}C_b^4 - 4.05\text{x}10^{10}C_b^3 + 12200C_b^2 - 0.0012C_b + 5.63\text{x}10^{-11} \tag{27}$$

2.4 Results and Discussion

Using each of the three approaches, the drop in formaldehyde concentration over time was initially tested in Excel before the reaction rates were implemented in the CFD model. For each of the three approaches, the drop in formaldehyde concentration over time was estimated in

Excel by using the appropriate Equation (21, 25, 26, and 27). Starting at time zero, the drop in formaldehyde concentration after 1 s was calculated. A time step of 1 s was selected since the rate of reaction was developed to give the change in formaldehyde concentration for a per second of time basis. Then the new concentration at time t = 1 s was calculated by using the following equation:

$$C_{t2} = C_{t1} - (rate)time \tag{28}$$

Equation 28 is a first order algebraic equation (difference form) of the differential equation for a batch reactor, $r_b = \frac{dC_b}{dt} = F(C_b)$. Then, using the new concentration at time t = 1 s the rate of formaldehyde decomposition was recalculated, again for a time step of 1 s to give the concentration at t = 2 s. This procedure was repeated for a total time of 3 hours (or 10800 seconds). The final results were then compared to the experimental results of Shiraishi et al., (2005b). The results of the Excel tests are shown in Figure 8.

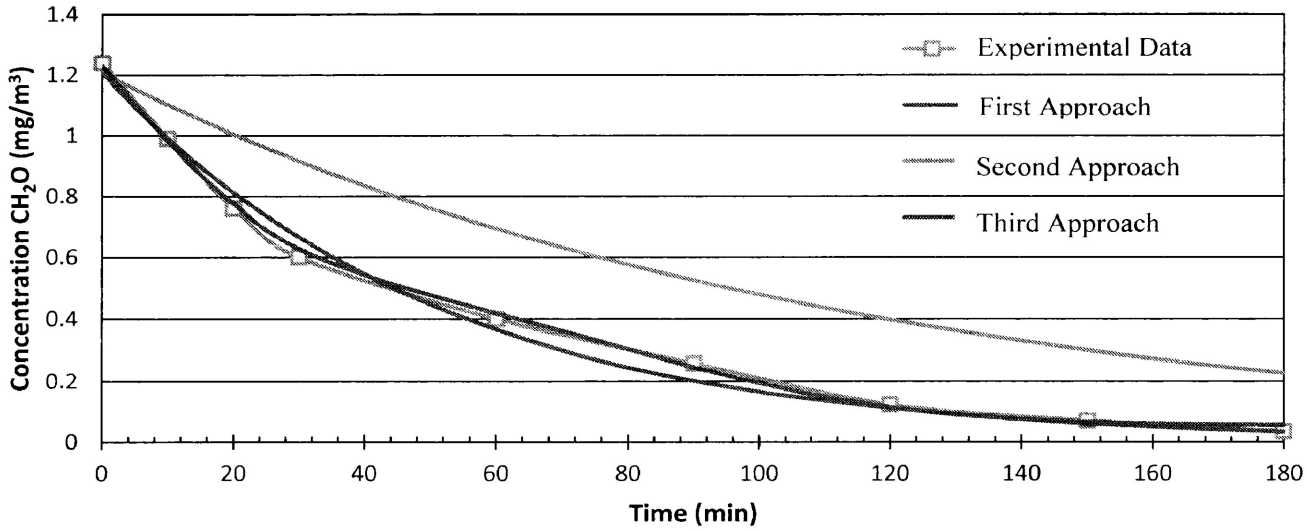

Figure 8: Comparison of various mathematically predicted kinetic model results

By first using Excel to mathematically predict the drop in formaldehyde concentration, it was possible to determine which of the three approaches were the best option when modeling the process using CFD and which approaches were not accurate and could be eliminated. It was apparent that the first approach (using the experimental kinetic model) was the least accurate of the three and did not accurately define the rate of formaldehyde decomposition. By first using

Excel to mathematically predict the drop in formaldehyde concentration the first approaches could have been eliminated as an option when modeling the PCO system using CFD. For this research, all three approaches have been modeled using CFD in order to demonstrate the point that (1) Excel can be used to eliminate inaccurate reaction rate models and (2) that the experimental reaction rate models cannot accurately predict the rate of reaction at the catalyst surface. Both approaches 2 and 3 (the exponential and polynomial kinetic models) predicted formaldehyde concentrations that were in agreement with the experimental results reported by Shiraishi et al., (2005b) with the third approach being the most accurate of the two.

Excel cannot be used alone to determine if the reaction rate model is accurate because it cannot reveal if there are any interferences. In this case, mass transfer limitations might also be present within the system since kinetics are only one part of the solution. The entire system must still be considered to obtain an accurate solution since both kinetics and hydrodynamics would affect the overall drop in formaldehyde decomposition. Excel cannot account for any mass transfer limitations due to the flow of air through the bulk of the reactor, which would be affected by the fan, turbulence, as well as the system geometry. For that reason, an integrated CFD model was still required to obtain a complete solution that considers all factors affecting the overall rate of formaldehyde decomposition.

2.4.1 General CFD Model Results

Figure 9 shows the path of the air through the bulk of the system. It shows that there was good movement of the air through the bulk of the system and there does not appear to be any zones of low mixing, which would have introduced mass transfer problems. These results indicate that there were no mass transfer limitations present in the bulk of the system and so the CFD model results should be in good agreement with the Excel results. This is not surprising since the system in this case was acting as a batch reactor where the hydrodynamics of the system are very well established. In a batch reactor, it is generally assumed that the fluid is perfectly mixed, meaning that the concentration profile should be fairly uniform throughout the entire system. It also means that there are no hydrodynamic issues throughout the system, such as zones of low mixing.

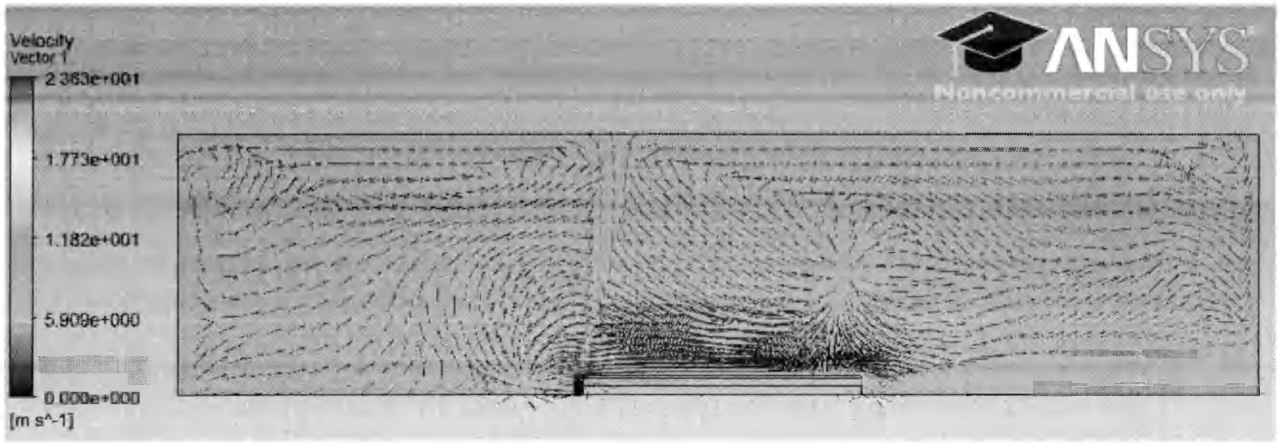

Figure 9: Flow path of the air through the system

The concentration profile of formaldehyde throughout the system can be seen in Figure 10. The air in the bulk of the system had a higher concentration of formaldehyde than the treated air leaving the reactor and so the air on the right hand side of the system, closest to the reactor outlet, had a slightly lower concentration of formaldehyde than the air on the left hand side of the system, closest to the reactor inlet. As the treated air exited the reactor on the right, it was recirculated back into the bulk of the system where it was mixed with the air in the bulk of the system.

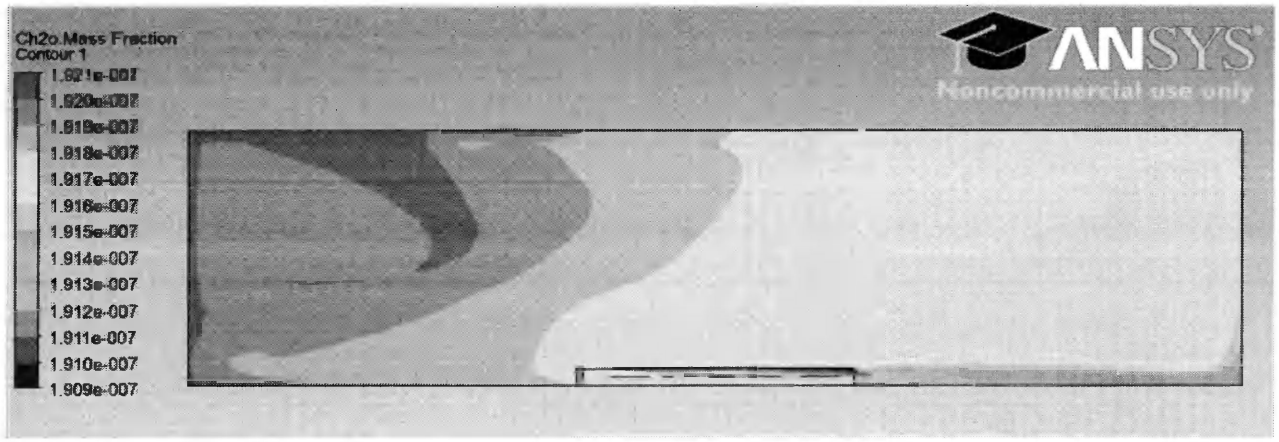

Figure 10: Concentration profile for formaldehyde throughout system after 3 hours

This effect is better demonstrated in Figure 11 which overlays the streamline path of the air onto the formaldehyde concentration profile for the bulk of the system. This shows how good mixing in the bulk of the system results in a fairly uniform concentration of formaldehyde throughout

the bulk of the system, again indicating that this system did not show any signs of mass transfer limitations throughout the bulk of the system that would affect the overall rate of formaldehyde decomposition.

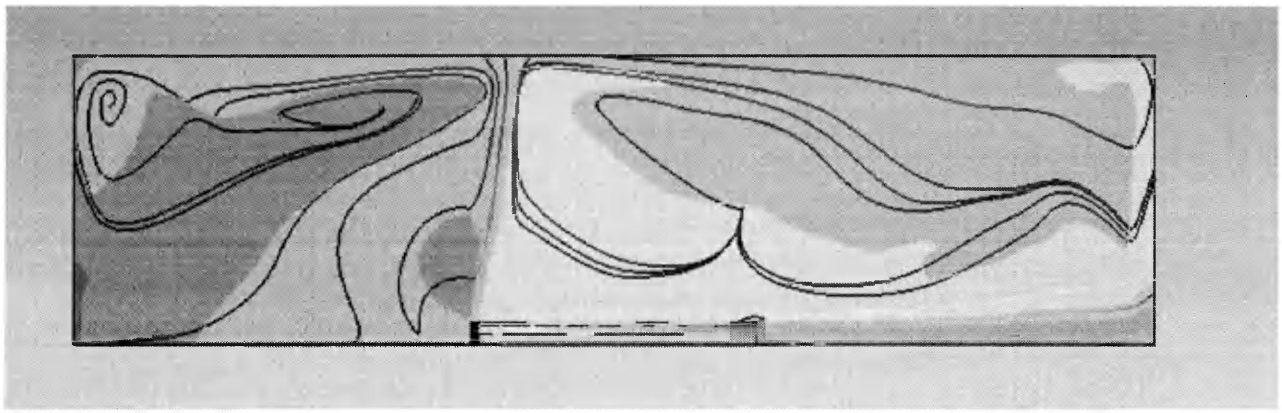

Figure 11: Streamline path and concentration profile through the bulk of the system

The drop in formaldehyde concentration across the catalyst surface can be seen in Figure 12. As the air travels to the right, along the catalyst surface, the concentration of formaldehyde at the surface decreases. Readings taken from the modeling software give concentration variations of formaldehyde across the catalyst of 1.918×10^{-7} kg/kg at the inlet and 1.913×10^{-7} kg/kg at the outlet. Using CFD, it is possible to see exactly how much of the contaminant is being removed with each pass through the reactor. This is important since in real life, the PCO reactor would not necessarily be within a closed system. In a home there would be multiple rooms connected onto the same air duct line transporting air from one room to the next.

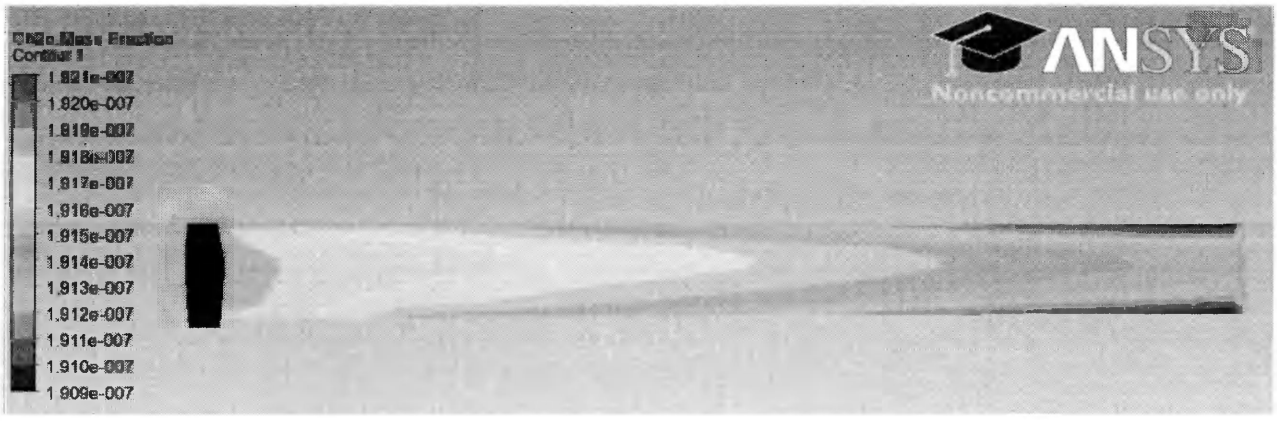

Figure 12: Concentration profile for formaldehyde along the reactive surface

2.4.2 CFD Modeling Using the First Approach

Comparing Figures 8 and 13 the results from both the Excel tests and the CFD models were very similar. This is mainly due to the fact that this system behaves as an ideal batch reactor with no mass transfer limitations. The behavior of a perfectly mixed batch reactor is well known and so it is easily modeled using CFD software. In this case, the PCO system is behaving as a perfectly mixed batch reactor, which was demonstrated in Figure 11. The CFD model results showed very similar results to those predicted using Excel (within 10%). In this case the hydrodynamics within the system were very well known and the rate of reaction only contained one variable, formaldehyde concentration. So, it appears that the initial conclusion from the flow path, that there does not appear to be any mass transfer limitations present in the system, was correct. This would have also been due to having sufficient turbulence in the system, ensuring that the rate of reaction was not mass transfer limited. However, this will not always be the case, and so it should not be assumed that Excel results will exactly match those obtained using CFD models.

As expected, the results from the first approach, using the experimental apparent reaction rate presented by Shiraishi et al., (2005b) were much lower than the actual rate of reaction on the catalyst surface. This was due to the fact that the experimental reaction rate was a combination of reaction kinetics and mass transfer effects, so, the CFD model was considering the mass transfer effects twice. This verifies the initial assumption that experimental reaction rates cannot be used to accurately describe the actual rate of reaction on the catalyst surface.

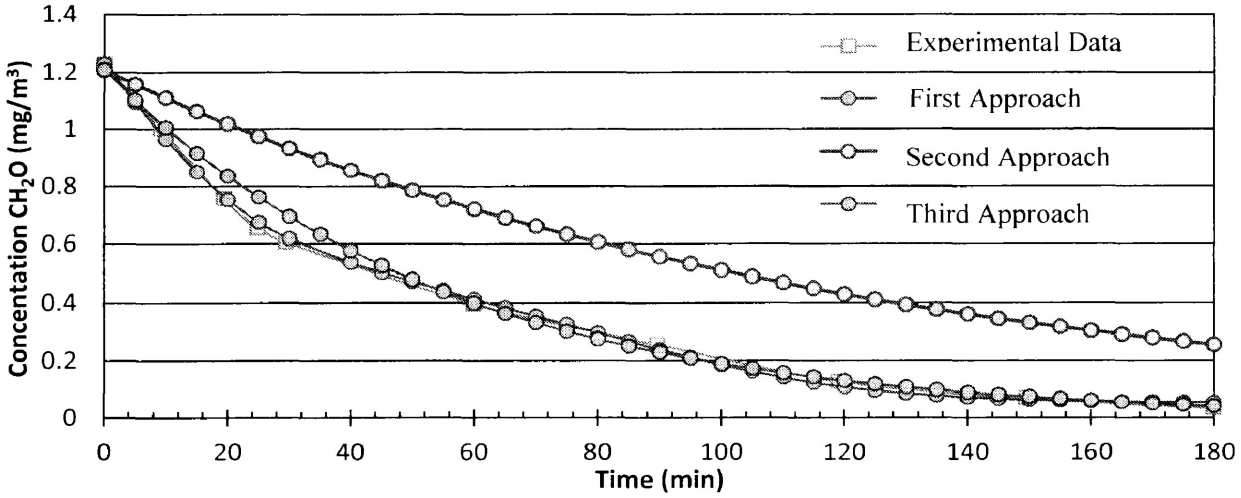

Figure 13: Comparison of the CFD results using three different approaches.

To prove that the reaction was not mass transfer limited the turbulent Schmidt number, Sc_t, was increased in order to increase the turbulence, and the mixing, in the system. This would have reduced any mass transfer limitation present throughout the system and along the surface of the catalyst. After increasing the Sc_t value several times the results showed no significant effect on the rate of reaction, Figure 14. This would indicate that the new approach resulted in a rate of reaction that was in fact independent of the mass transfer effects and that the default Sc_t value of 0.7 was sufficient in this case.

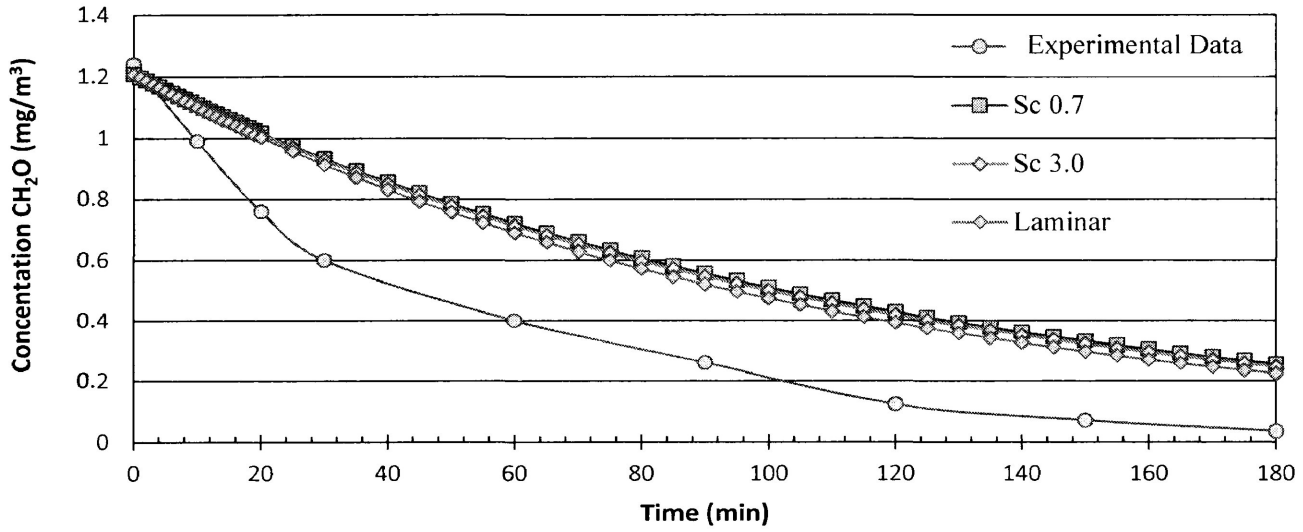

Figure 14: CFD model results using different Sc values

2.4.3 CFD Modeling Using Second Approach

Using the second approach of an exponential kinetic model, the CFD model results were more consistent with the experimental results reported by Shiraishi et al.,(2005b). Similar to the experimental results, the concentration of formaldehyde dropped at a fairly constant rate for the first 30 min, after which the rate of formaldehyde decomposition began to decrease. It can also be seen in Figure 13 that the model results show slightly higher concentrations than the reported results within the time frame of 15 – 40 min. It appears that the experimental results show a much sharper shift in the rate of decomposition after the initial reaction period, while the exponential rate function produces a more uniform shift in the rate of reaction after the initial reaction period. These results do verify that for a closed system (behaving as a batch reactor), an exponential kinetic model could be used to predict PCO kinetics in a CFD model over a long

period of time, but it is not as accurate at predicting the initial drop in the formaldehyde concentration.

2.4.4 CFD Modeling Using Third Approach

Using the third approach of a polynomial reaction kinetic model the CFD model results did match the reported experimental results as can be seen in Figure 13. This third method was able to accurately predict the initial drop in formaldehyde concentration and the drop in concentration over time. When all three approaches were compared together with the experimental results, the third approach gave the best results for predicting the drop in formaldehyde concentration over time. This was due to the separation of the initial rate of reaction. By recognizing that the initial rate of reaction will be greater than the rate of reaction after the initial period a more precise reaction model was developed for the initial period. Unlike the exponential model, with a two part rate model each of the two parts can be individually adjusted in order to best match the experimental results. For example, if the initial rate is too low it can be increased by a factor till it matches with the experimental results.

2.5 Conclusions

Using the new approach discussed in this section, the experimental kinetic model for formaldehyde decomposition was adapted to reflect surface reactions based on VOC levels on the catalyst surface. By considering the reacting volume as only a thin layer of cells just above the catalyst surface, the reaction rate expressions became dependent solely on the concentration of formaldehyde at the surface, as opposed to the bulk concentrations. This meant that the change in concentration that was being calculated using the UDF codes was only affected by the reaction kinetics, unlike the experimental reaction rates that were based on the bulk concentrations, which were dependent on both reaction kinetics and mass transfer effects.

A complete CFD model was developed for the system considering hydrodynamics, species transport, and reaction kinetics, and the results were in agreement with the experimental data that was reported by the author. It was determined that a two part polynomial rate expression was the most accurate as it was able to account for the higher initial rate of reaction. However, the exponential model did give reasonable results as well due to the closed system behaving like a batch reactor.

The complete CFD model showed how engineers can use CFD to optimize system design by analyzing the flow path of the air through the system. The CFD model also showed that the closed system did behave as a batch reactor with perfect mixing and a fairly uniform concentration of formaldehyde throughout the bulk of the system.

Chapter 3 – Versatility of Method of Reaction Modeling

The versatility of the proposed new method for reaction modeling is demonstrated by using the same approach from the previous section to develop a reaction rate model where the rate expression was controlled by two variables: the VOC concentration and the UV irradiance level at the catalyst surface. In order to describe the complete surface mechanism happening on the catalyst surface the reaction rate should be able to account for variations in the UV irradiance levels. The UV irradiance rate is the main governing factor in the photocatalytic reaction rate. Additionally, irradiance levels can vary dramatically across a surface due to the effects of shadowing on the catalyst surface, or in the case of multiple lamps overlapping of the radiation fields. As a result the surface reaction is dependent on the rate of UV irradiance at each point along the reacting surface.

The work of Brosillon et al., (2008), which studied the decomposition of butyric acid in air using a PCO system, was modeled. Using the method developed in the first case, the experimental reaction rate was adapted to reflect the true rate of reaction at the catalyst surface which is dependent on both butyric acid concentration and the UV irradiance level on the catalyst surface.

3.1 Theory

3.1.1 Radiation Model

Radiant distribution energy can be calculated using the radiative transport equation:

$$\frac{dI(r,s)}{ds} + (a + \sigma_s)I(r,s) = an^2\frac{\sigma T^4}{\pi} + \frac{\sigma_s}{4\pi}\int_0^{4\pi} I(r,s)\Phi(s * s')\,d\Omega' \qquad (28)$$

Where r is the position vector

s is the direction vector

s' is the scattering position vector

α is the absorption coefficient

σ_s is the scattering coefficient

n is the refractive index

T is the temperature of the air

and Ω' is the solid angle

The lamp location with respect to the catalyst surface is a crucial step in the design of the PCO system in order to achieve a uniform irradiance level across the catalyst. Calculating radiation fields for different reactor configuration and lamp types showed that the general assumption made in lab experiments of having a uniform radiation field across the catalyst is not generally correct.

3.1.2 Discrete Ordinates (DO) Method

There are several different models that can be used to solve the radiative transport equation. In this case the DO method was used to model the UV radiation. The DO method has the advantage of being the most versatile of the radiation models. It is not restricted by the optical thickness and can be used to solve a wide range of radiation problems. The DO method solves the radiative transport equation by dividing each cell into a finite number of discrete solid angles, s (Figure 15).

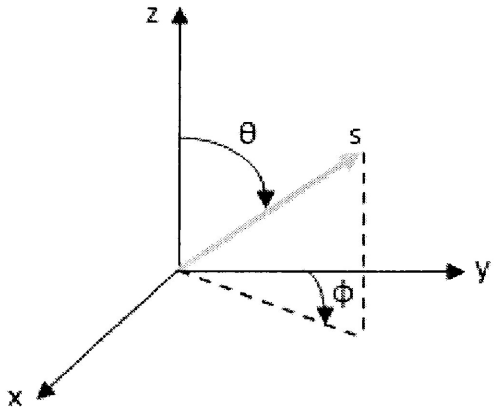

Figure 15: Solid angle division for DO method

Similarly to how the conservation equations are solved for a finite number of cells, the DO method solves the radiative transport equation for each discrete solid angle transforming equation (28) into:

$$\nabla(I(r,s)s) + (a+\sigma_s)I(r,s) = an^2\frac{\sigma T^4}{\pi} + \frac{\sigma_s}{4\pi}\int_0^{4\pi} I(r,s)\,\Phi(s*s')d\Omega' \qquad (29)$$

3.1.3 Reaction Rate Model

Brosillon et al., (2008) proposed a reaction model, which describes the interdependence of UV photon flux and the butyric acid concentration. It is this reaction rate model that was used to describe the rate of butyric acid decomposition in the CFD model. They chose to look only at the initial rate of reaction because it is closest to the intrinsic reaction rate as it is only the butyric acid reacting and there is no concern of by-products competing for active sites and hindering the rate of reaction.

$$r_4 = \frac{\beta I}{1+\gamma I+xC_B} C_B \tag{30}$$

Where r_4 is the rate of reaction

I is the UV irradiance at the catalyst surface

C_B is the butyric acid concentration in the bulk of the system

and β, γ, and x are rate constants.

The experimental data was evaluated using nonlinear regression to solve for β, γ, and x in Excel and the following expression was obtained where C_s is the concentration of butyric acid at the catalyst surface:

$$r_o = \frac{9.44314e^{-11}I}{1+0.31818*I+0.004160567*C_s} C_s \tag{31}$$

3.1.4 Hydrodynamic and Turbulence Models

For a detailed description of the theory for the turbulence and hydrodynamic models see section 2.2.2 and 2.2.3.

3.2 Second Case Study

3.2.1 Geometry Model and Mesh Structure

The reactor setup was based on the reactor system described by Brosillon et al., (2008). The PCO system is made up of an annular reactor (r_i = 14.25 cm) shown in Figure 16. The photocatalytic material (non-woven paper coated in TiO_2/SiO_2) covers the inside walls of the reactor (SA = 0.3043 m^2) as well as a pierced cylinder in the center of the reactor (SA = 0.0567 m^2). There were also 12 UV lamps (λ_{max} = 365 nm) mounted between the two catalyst surfaces.

The fluid passage inside the reactor was divided into 667,544 infinitesimal cells (mesh) to establish a mesh independent solution. The reactor configuration is symmetrical, so, in order to reduce the computation time one quarter of the reactor system was modeled.

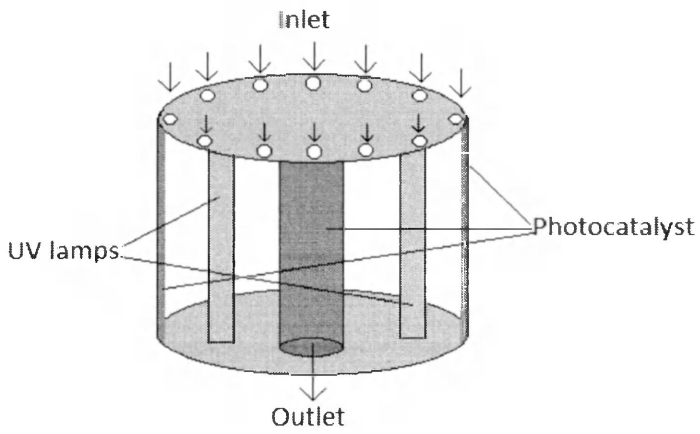

Figure 16: Reactor Setup for the second case

3.2.2 Operation and Boundary Conditions

Ansys Fluent 14.0 was used to model the reactor system. Brosillon et al.,(2008) stated that they had verified through experimental analysis that their system was under turbulent flow conditions, so, the $k - \epsilon$ method was used to model the turbulent flow within the system. To model the flow through the inner catalyst filter the interior of the filter media was set as a "porous jump". The "porous jump" boundary condition is a 1D simplification of the porous media model which is used to model pressure drops through screens and filters. The "porous jump" condition produces more accurate results for the simpler media since these do not experience a high enough pressure drop to drive the flow. The filter was modeled using data from (Taranto et al., 2009) for the pressure drop across a near identical filter (permeability 0.00022 m^2, pressure-jump coefficient 0.013714 m^{-1}) for a variety of flow rates under similar flow conditions.

The inlet species concentrations were set as boundary conditions. Since the initial concentration of butyric acid is so low (192 – 576 mg/m^3) the physical properties of the contaminated air remain constant as the reaction progresses. The properties of the contaminated air mixture were set to those of air at 25°C and average indoor air concentrations for O_2 (20 % by volume), H_2O (RH 30%), and CO_2 (340 ppmv) were used. The multicomponent mass diffusivity was selected

and the values for each of the species combinations were calculated for a gas-gas system(Treybal, 1980).

The rate of reaction on the surface of the catalyst was developed (see Theory section 3.1.3) using external codes (macros) and integrated into the mass conservation equations for each reacting species. The reaction rate expressions were introduced to the model as source terms (S_i from Equation 10) using user defined functions (UDFs).

The radiation field was modeled using the DO method. The lamp faces were set to semi-transparent and the diffused radiation levels were initially set to give an area weighted average irradiance level on the outer catalyst wall of 7 W/m^2, which was the lowest irradiance level tested by Brosillon et al., (2008). The irradiance level was later increased to give an area weighted average irradiance level of 8.77, 10.5, 12.2, and 14 W/m^2 on the outer catalyst wall, which were the other irradiance levels tested by Brosillon et al., (2008). The authors stated that they measured the irradiance level at various locations across the catalyst wall and used the average value to establish the reaction rate model. It was assumed that the absorbance and scattering effects were negligible and that the radiation field is unchanged throughout the reaction.

3.2.3 Solution Setup

The SIMPLE discretization scheme was selected using the pressure based solver for steady-state conditions. The default discretization methods were used for solving the conservation equations. The solution residuals were set to $1e^{-4}$ for hydrodynamic elements, $1e^{-8}$ for species mass fractions, and $1e^{-6}$ for the DO calculations. In this case it was determined that a higher residual was required for the species mass fractions in order to obtain accurate results.

The system was set up for standard room conditions (25°C and 1 atm). The initial system conditions were established before the source terms were introduced. The inlets were set as a "velocity inlet" and the outlet was set as "outflow". The inlet velocity was adjusted to give an outlet velocity of 0.189 m/s which matched the flow rate used by Brosillon (2008). To establish the species distribution the inlet mass fractions for butyric acid, O_2, CO_2, and H_2O were set as boundary conditions. Once the initial conditions were established the source terms were introduced to the catalyst surfaces for each of the reacting species.

It is important to note that the radiation model is designed based on thermal radiation. In order to eliminate any interference of thermal radiation on the UV radiation the temperature was set to 1 K in all cell zones within the system when solving the radiation model. If this step is not done, then all irradiance levels measured will be a combination of both thermal and UV radiation.

3.3 Results and Discussion

Microsoft Excel software was used to calculate the rate constants β, γ, and x for equation 31 using the nonlinear regression solver. The values of the rate constant were optimized in order to minimize the % error between the calculated reaction rate and the experimental reaction rate with the final constant values found in table 2. Looking at the denominator in equation 31 it appears that the UV irradiance level is in fact the dominating factor over the butyric acid concentration since $\gamma I >> \chi C_s$. This is in line with the PCO kinetic theory which states that the UV irradiance is the governing factor in PCO reactions.

Table 2: Constant values for equation 31

β	γ	X
9.44314×10^{-11}	0.31818	0.004160567

The final results of the nonlinear regression can be seen in Figure 17. The final solution results gave calculated reaction rates within ± 8 % of the reported experimental reaction rates, with the exception of the case of the initial butyric acid concentration of 576 mg/m^3 (± 24%). An initial concentration of 576 mg/m^3 is well outside the range of butyric acid levels that would be found in indoor air. This level (576 mg/m^3 or 609 ppbv) is also well above the odor threshold for butyric acid (240 ppbv). Since butyric acid gives off a very strong and unpleasant odor anything above the recommended threshold would not be tolerable. For this reason the case of C_o = 576 mg/m^3 was not considered in the CFD model tests.

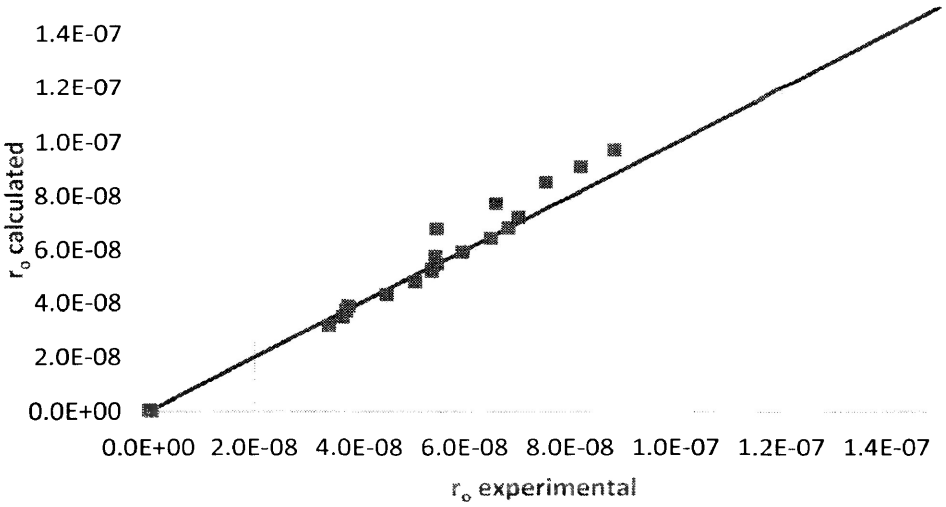

Figure 17: Linear regression results

Using equation 31 the initial rate decomposition for different initial butyric acid concentrations over a range of UV intensities was first tested in Excel as shown in Figure 18. For the first three butyric acid concentrations the results were within 5% of the experimental results. For the final butyric acid concentration of 576 mg/m^3 the results were within 10-24% of the experimental results. Since a butyric acid concentration of 576 mg/m^3 is well outside the range that would be found in indoor air this concentration was not considered when running the CFD models and so these results were acceptable. These results indicated that equation 31 should be able to predict the initial rate of reaction for different initial butyric acid concentrations and irradiance levels when implemented in the CFD model.

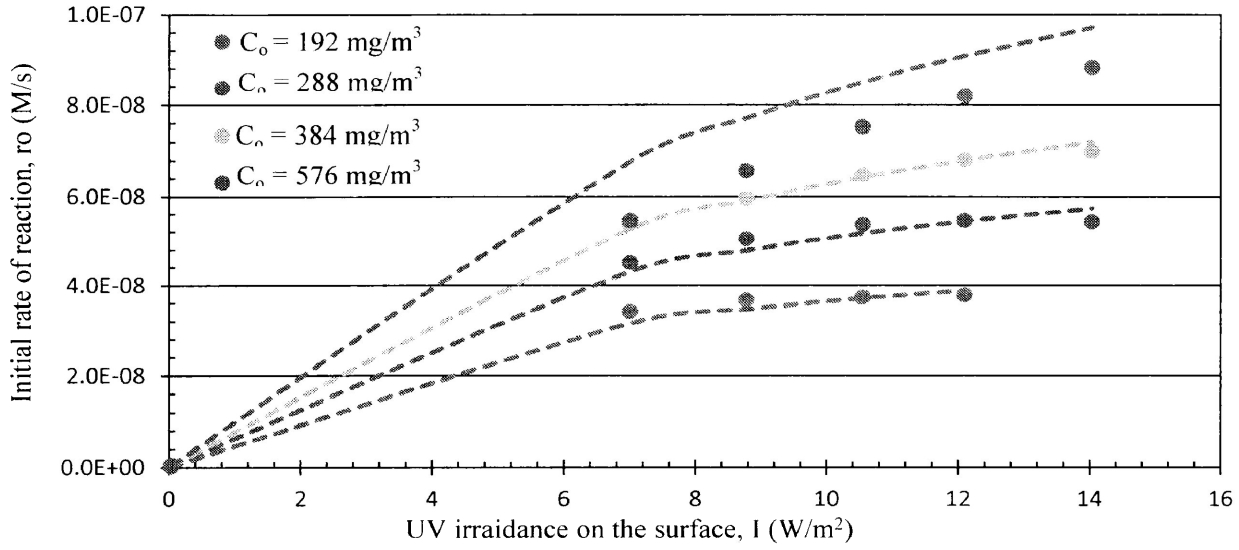

Figure 18: ro vs I experimental data (o) and predicted values using Excel (- - -)

Again, as outlined in the first case this was done in order to determine if the new reaction rate model would predict the rate of butyric acid decomposition comparable to the experimental results. Using Excel it was determined that the reaction rate model results are in good agreement with the experimental results. Again, it should be noted that Excel alone cannot determine if the reaction rate expression is accurate. In this case, Excel could not account for fluctuations in the UV irradiance level along the catalyst surfaces or determine if there are any mass transfer effects within the bulk of the system. A complete CFD model was still required in order to account for all parameters that may impact the overall decomposition of butyric acid since that is what was compared with the experimental results.

3.3.1 CFD Model Results

As the air entered the reactor above the outer catalyst wall, it flowed along the wall and through the internal catalyst filter where it finally exited through the outlet on the right side as shown in Figure 19. The streamline path indicates that there could be a zone of low mixing at the left end of the catalyst filter since most of the air is passing through the bottom half of the filter. A zone of low flow could cause some issues if this reactor configuration were tested at full scale. The problem area could cause mass transfer limitations through the bulk of the system and the air could become stagnant in this section of the reactor. Also, over time it could cause early fouling

of the catalyst filter which would result in a shorter life span for the catalyst filter if the system is treating higher molecular weight or more complex contaminants which produce intermediates. The production of reaction intermediates that are not easily decomposed is the leading cause of catalyst fouling, and if these intermediates are not removed from the catalyst at a sufficient rate they will build up on the surface of the catalyst which would dramatically reduce the effectiveness of the catalyst and the overall performance of the PCO system.

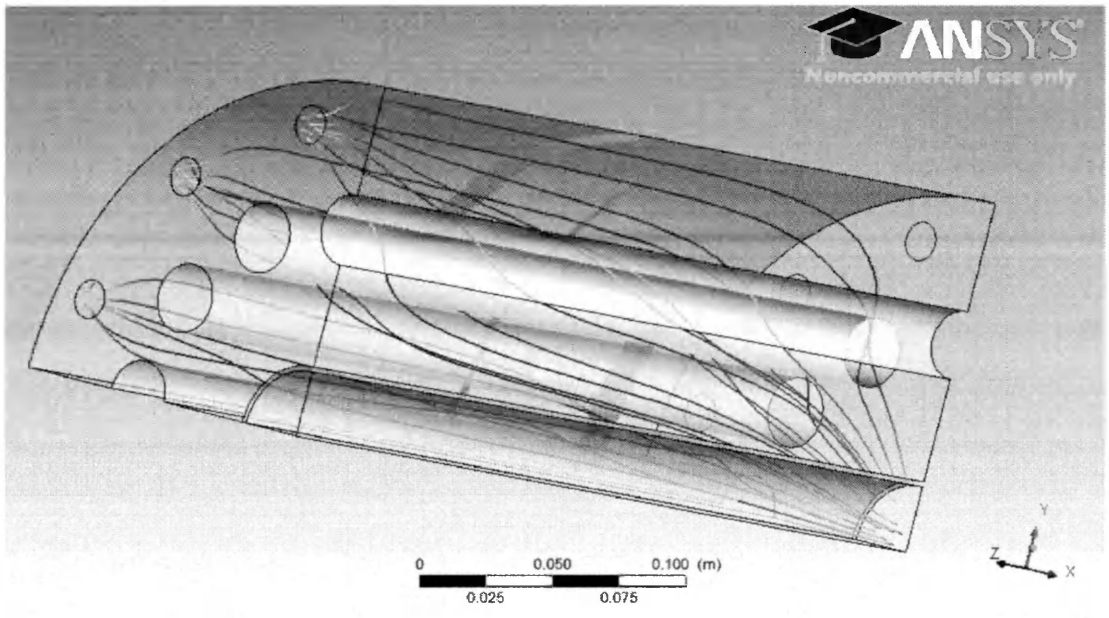

Figure 19: Streamline path of air through reactor

Examining the species distribution along the catalyst surfaces, Figure 20, the drop in butyric acid across the catalyst surfaces can be seen. As would be expected the butyric acid levels dropped from left to right across the catalyst surfaces following the flow path of the air. Overall, there was a larger drop in the butyric acid concentration along the outer catalyst wall which would be expected since, as seen with the streamlines, the air passes more time over the outer catalyst wall than along the inner catalyst filter. Also, the air traveling through the filter had already been partially treated along the outer catalyst wall which could also account for the smaller variation in butyric acid levels along the inner catalyst filter.

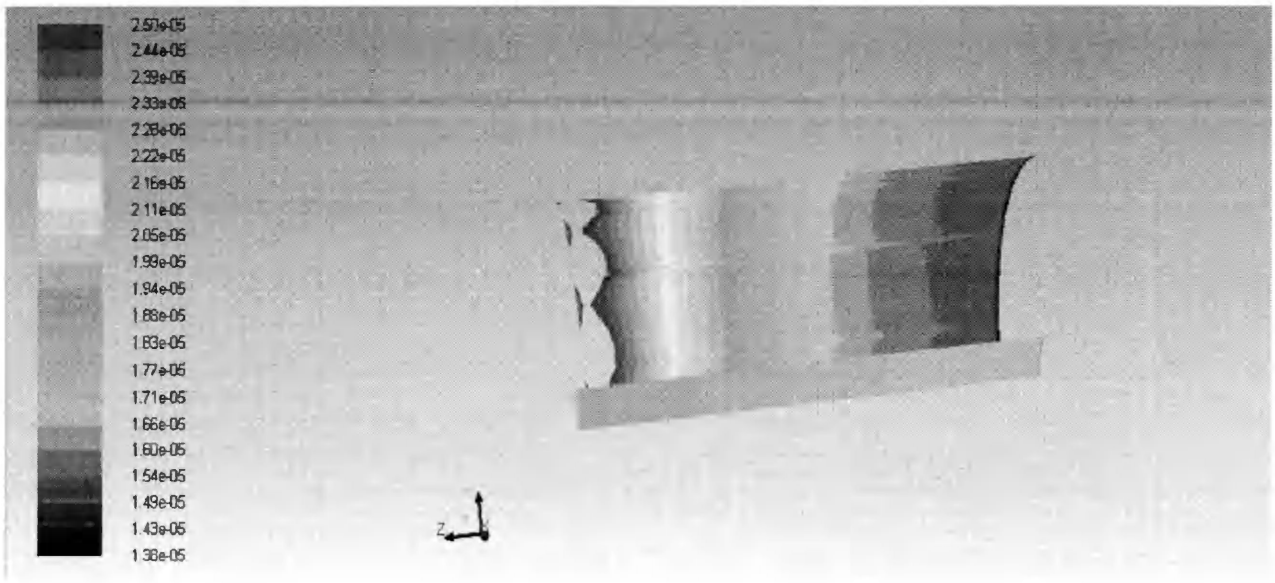

Figure 20: Specie distribution of butyric acid along the activated catalyst surfaces

The initial rate of decomposition of butyric acid was predicted for initial concentrations of 192, 288, and 384 mg/m^3 at UV irradiance levels of 7, 8.77, 10.5, 12.2 and 14 W/m^2, Figure 21. For all three initial butyric acid concentrations the rate of decomposition was over estimated (20 – 49 %) for the various UV irradiance levels and it appears that the rate of reaction has already reached steady state. In this case steady state refers to the effect of UV irradiance levels on the rate of reaction. For all three concentrations there was no increase in the rate of butyric acid decomposition as the UV irradiance level was increased from 7 W/m^2 up to 14 W/m^2. In real life this would indicate that the catalyst surface is saturated with radiation energy (producing enough electron-hole pairs) at 7 W/m^2. Above the point of saturation the system becomes inefficient in terms of energy usage since the catalyst is either producing excessive electron-hole pairs or not absorbing the energy at all. However, the experimental results show that the rate of reaction should still be increasing with UV irradiance levels and so the catalyst surface is not saturated.

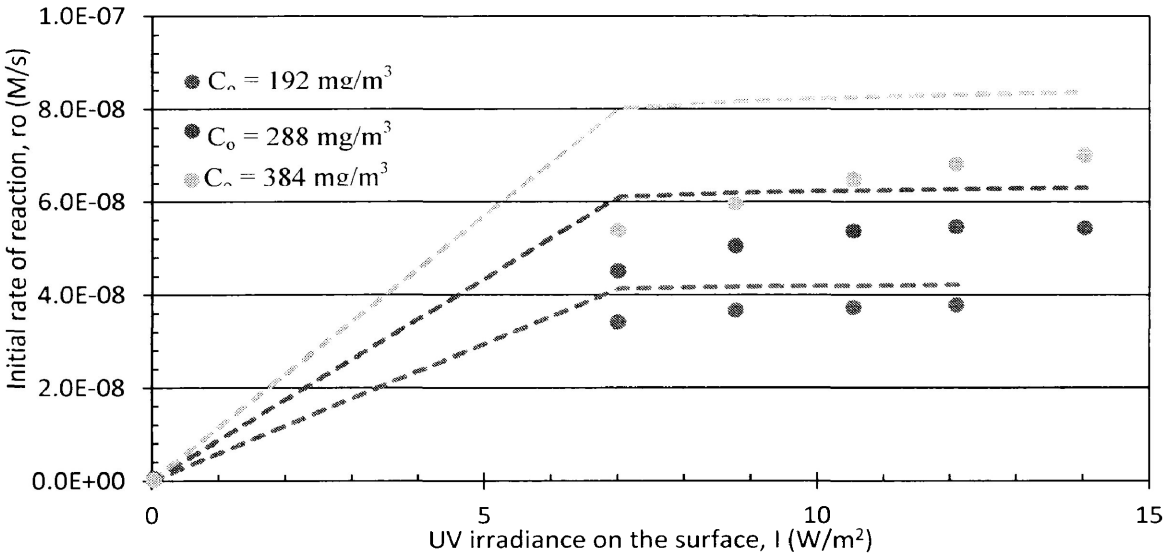

Figure 21: Comparison of CFD model results (---) with experimental data

This could be due to the general assumption that the UV irradiance is uniform across the catalyst surface. However, from examining the radiation field of the CFD model it was noted that the radiation field across the catalyst surface was not entirely uniform. The levels were most concentrated across the center of the reactor and then dropped towards the two ends of the reactor, Figure 22. By assuming that the UV irradiance levels would be uniform across the catalyst surface the rate of reaction was initially over estimated in Excel since the rate of decomposition at the ends of the reactor would have been lower than across the center of the reactor. This demonstrates why Excel alone is not a good indicator of whether the rate expression is accurate.

In order to get an accurate average of the UV irradiance on the catalyst surface the levels should be measured across the entire surface at even intervals with as many readings as possible. If Brosillon et al.,(2008) did not take sufficient UV readings at the ends of the reactor then the levels being reported would have been slightly higher than the actual UV irradiance.

Looking at Figure 22, it can be seen that the irradiance levels at (a) the two ends of the catalyst wall were around 4.2 W/m^2 while in the center of the catalyst wall the irradiance levels were around 8.27 W/m^{2}and (b) at the two ends of the catalyst filter the UV irradiance levels were around 11W/m^2 while at the center of the catalyst filter the irradiance level were around 23 W/m^2. This indicates that the irradiance levels at the two ends of the catalyst surface were only

half of that found in the center of the catalyst. This was not consistent with the assumption that the irradiance would be uniform across the catalyst. This can be explained by the fact that the UV radiation will diffuse away from the lamp uniformly in all directions, however, at the ends of the catalyst it is only the UV light from the ends of the lamp that will reach the catalyst. In the center of the catalyst UV radiation from the entire length of the lamp is able to reach the catalyst and so it will be receiving a higher UV dose of UV radiation which results in higher irradiance values. Since Brosillon et al.,(2008) did not state where the irradiance levels were measured we were left to assume that their readings were overestimating the irradiance levels across the catalyst by not taking sufficient readings at the ends of the catalyst.

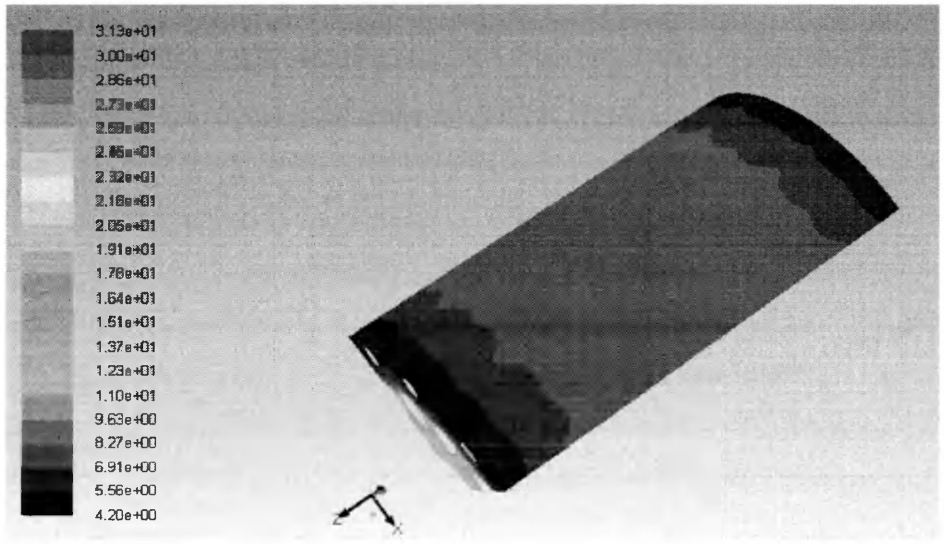

(a)

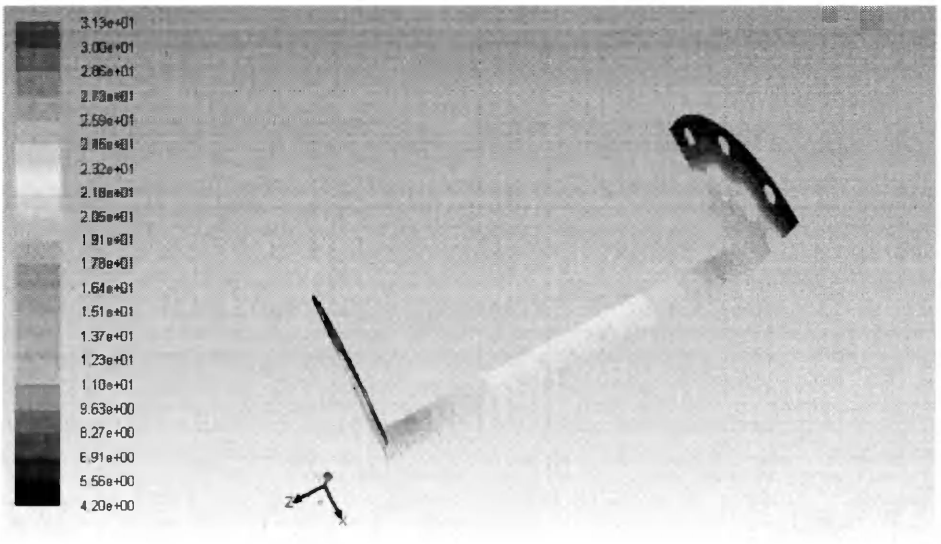

(b)

Figure 22: Irradiance (a) across the outer catalyst wall, and (b) throughout the system

3.3.2 CFD Results Using Adjusted Rate of Reaction

For the second set of runs the rate of reaction was reduced by a factor of 0.5 to account for large variations in the UV irradiation levels across the catalyst surface. Using the reduced reaction rate model the CFD model results were much closer to the experimental results as can be seen in Figure 23. In this case the model results were within 2 – 15 % of the experimental results which is a good agreement. Due to lack of information regarding the experimental setup for this case, several assumptions were made that may not fully compare with experimental conditions. This can explain the observed deviation between CFD model and experimental results. It also shows that the rate of decomposition of butyric acid does not immediately reach steady state.

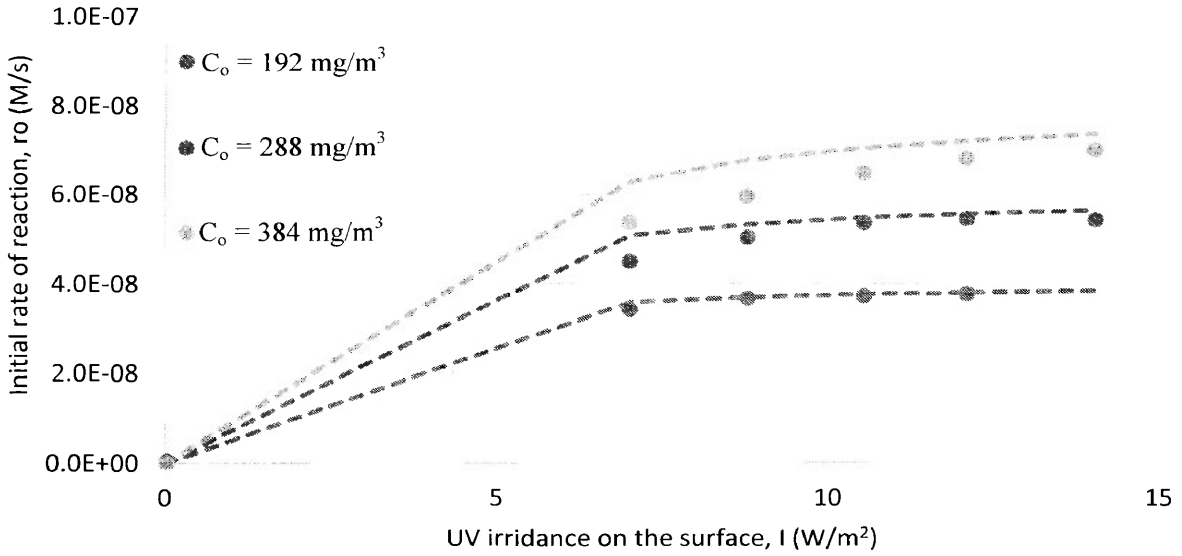

Figure 23: Model results (---), experimental data (*)

3.4 Conclusions

As seen in the previous case, the experimental reaction rates cannot be directly implemented into the CFD model for modeling the complex surface reactions. In this second case, using this novel approach the reaction rate model was able to predict the rate of decomposition for butyric acid in the air for a variety of initial concentrations and UV irradiance levels at the catalyst surface. The initial CFD model results were off by 20 – 50% due to overestimation of the initial reaction rate due to the variations in UV irradiance levels across the reacting surface. The variations in the UV irradiance also demonstrated why Excel is not a good indicator the overall rate of butyric

acid decomposition since it cannot account for any mass transfer limitations or variations in the radiation levels that would impact the rate of decomposition.

The CFD model results also disproved the general assumption that the UV irradiance levels are uniform across the catalyst surface. The UV irradiance levels can vary greatly across the length of the catalyst surface and so sufficient readings must be taken across the entire catalyst surface in order to obtain an accurate average of the UV irradiance. If not the resulting rate of reaction would be overestimated (or underestimated) as seen in this case.

After examining the streamline paths for the air through the reactor system, it became apparent that there would be a zone of low mixing at one end of the catalyst filter due to most of air passing through the bottom half of the filter. This could result in a drop in reactor performance and possibly a shorter life span of the catalyst if this reactor configuration was run at full scale.

Chapter 4 – Applications

4.1 Optimize PCO System Design

Using the new approach to modeling surface reactions that has been outlined in this work, researchers can obtain a better understanding of how VOC levels are actually changing on the surface of the catalyst. As demonstrated in the first case, this new approach provides more accurate reaction rate expression than the reaction rates obtained from experimental work. By defining the reaction rate expressions solely by what is happening at the catalyst surface, researches can compare the performance of different systems more accurately by comparing the PCO reactor performance as opposed to the overall performance of the entire system.

One area of study that this research could help to enhance is the research into different catalyst materials, as well as different catalyst support materials, since different reactor types or support material can experience different mass transfer and mixing effects through the bulk of each system which would affect experimental reaction rate expressions. It is difficult to accurately compare two systems, which will experience different mass transfer effects, to determine which of the two systems is more effective at removing the VOCs. Mass transfer effects within the bulk of the system can be adjusted to minimize any mass transfer limitations. So by using this CFD modeling approach, researchers can model the two systems and compare the results of what is happening on the catalyst surfaces to determine which system is truly more effective at treating the VOCs in the air.

Obtaining an accurate rate of reaction at the catalyst surface also allows for better optimization of the PCO system design. By converting the rate of reaction so that it describes only the interactions at the catalyst surface the rate of reaction is now independent of what of happening in the bulk of the system. Using the CFD model results to evaluate the mass transfer effects in the bulk of the system researchers can address any mass transfer concerns in order to improve the overall system performance. The performance of a system can be evaluated for changing internal geometry (mixing effect), flow rate, flow obstructions (such as support material), obstructions in the radiation field, etc.

Using this new approach to develop an integrated CFD model also offers the opportunity to predict how the PCO system would perform at full scale inside a home or office building. With experimental setups at full scale, there are many potential sources of error, mainly that VOC levels can be so low that it is difficult to obtain an accurate measurement. In order to achieve accurate measurements at full scale the initial VOC levels would need to be increased in order to obtain accurate measurements which would pose potential health risks for any individual present in the space. Using CFD to model the full scale setup, researchers can determine if the PCO system is capable of treating the contaminated air on a larger scale and also how much the system could handle. The same system could also be tested for several different applications (home, office building, library, kitchen, etc.) to determine which applications the system is best suited for. A simple case study was performed to show how the proposed new approach to reaction modeling developed in the thesis work could be used to estimate the performance of a PCO system in a room within a home.

4.2 Case Study

A case study was performed in order to demonstrate how this research could be used to predict the performance of a PCO in treating butyric acid within a closed room. The PCO system was enclosed within the air duct system in a closed room, as it would be in real life. The PCO system was tasked with treating air contaminated with butyric acid at typical levels found in indoor air to see how the system would perform when treating the contaminated air on a larger scale. The reaction rate expression obtained in the second case for butyric acid was used in this case study to model the rate of reaction at the catalyst surface. This case study also looked at the introduction of a constant point source of butyric acid. In this case, that point source represented one or two people emitting butyric acid at a constant rate.

4.2.1 Geometry Model and Mesh Structure

The system was modeled in 2D in order to simplify the design and reduce the computation time required. The closed room (2m high x 2m wide) with a cycling air duct system (0.295m x 0.2 m), as shown in Figure 24, was modeled. The dimensions of the air duct were selected to be within the size range for rectangular air ducts in a home (see Appendix F for common duct sizing for air ventilation systems). The air duct system contained a PCO system based on the design used in the second case. By containing the PCO system within the air duct there would be no

risk of UV exposure to skin. The PCO system consisted of 3 UV lamps (diameter 28 mm) mounted horizontally in front of a catalyst filter (thickness 2 mm). Inside the closed room was a chair which acted as the constant source of butyric acid, representing one or two people inside the room. A virtual fan was placed at the end of the air duct in order to produce the axial flow through the duct system. After using several different mesh numbers, the solution reached mesh independent results with a final mesh number of 157,753.

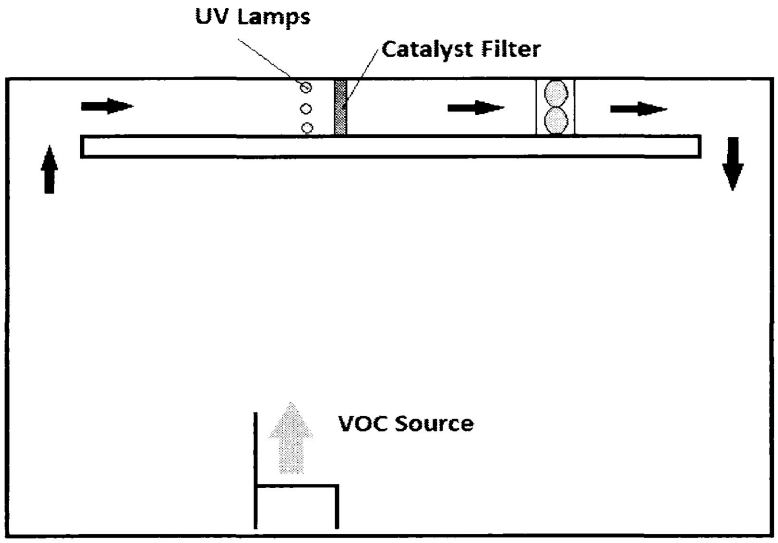

Figure 24: Case study system geometry

4.2.2 Operating and Boundary Conditions

Ansys Fluent 14.0 was used to model the reactor system. In order to achieve adequate flow through the air duct the air should be experiencing turbulent flow conditions (Re 3657 which is transitional flow) so the $k - \epsilon$ method was used to model the turbulent flow within the system. To model the flow through the inner catalyst filter the interior of the filter medium was set as a "porous jump". The filter was modeled using data from Taranto et al., (2009) for pressure drop across a near identical filter (permeability 2.2 e^{-4} m^2, pressure-jump coefficient 0.013714 m^{-1}) for a variety of flow rates under similar flow conditions.

The inlet species concentrations were set as boundary conditions. The initial concentration of butyric acid in the room was so low (1 ppmv, above the upper limit of the odor threshold for butyric acid) the physical properties of the contaminated air would remain constant as the

reaction progresses. The properties of the contaminated air mixture were set to those of air at 25°C and average indoor air concentrations for O_2 (20 % by volume), H_2O (RH 30%), and CO_2 (340 ppmv) were used. The multicomponent mass diffusivity was selected and the values for each of the species combinations were calculated for a gas-gas system (Treybal, 1980).

The radiation field was modeled using the DO model. The lamp faces were set to semi-transparent and the diffused radiation levels were set to give an area weighted average irradiance level on the catalyst filter of 7 w/m^2. It was assumed that the absorbance and scattering effects were negligible and that the radiation field was unchanged throughout the reaction.

4.2.3 Solution Setup

The SIMPLE discretization scheme was selected using the pressure based solver. The default discretization methods were used for solving the conservation equations. The solution residuals were set to $1e^{-4}$ for hydrodynamic elements, $1e^{-8}$ for species mass fractions, and $1e^{-6}$ for the DO calculations.

The system was set up for standard room conditions (25°C and 1 atm). To establish the initial system conditions the model was run under steady-state conditions. The interior boundary of the fan was set as "FAN". By trial and error, the pressure drop was adjusted to 230 Pa across the fan in order to give an average velocity of 0.24 m/s across the catalyst filter and an average velocity of 2 m/s across the duct system, which falls within the range of acceptable air velocity for an air vent in a home (The Engineering Toolbox, 2014). To establish the species distribution the initial mass fractions for butyric acid, O_2, CO_2, and H_2O in the bulk of the system were set as boundary conditions.

It is important to note that the radiation model is designed for thermal radiation. In order to eliminate any interference of thermal radiation from UV radiation the temperature was set to 1 K in all cell zones within the system when solving the radiation model. However, all physical properties are used at ambient temperature. This technique does not result in interference with the conservation of mass and momentum and resolves the problem for the radiant energy conservation equation.

Once the initial conditions were established, the system was switched from steady-state conditions to transient and the reaction model was introduced to the catalyst surfaces for each of

the reacting species. The rate of reaction on the surface of the catalyst that was developed in the second case using external codes (macros) was used in this case study and was integrated into the mass conservation equations for all species. The reaction rate expressions were introduced to the model as source terms (S_i from Equation 10) using user defined functions (UDFs).

After determining how long the PCO system required to treat the contaminated air and reach steady-state the model was reset to the initial conditions and a constant source of butyric acid was introduced. This point source represented a person in a closed room while emitting butyric acid at a constant rate (1.9 mg/h/person is the average rate butyric acid is emitted from the human body (Cooper & Alley, 2011)).

4.3 Results and Discussion

4.3.1 PCO System with No Point Source

The initial test run of the CFD model was performed prior to introducing the constant source of butyric acid. This was to determine how long it would take the PCO system to reach steady state and at what concentration it would reach a steady state.

Figure 25 shows the concentration profile of butyric acid throughout the system. As the contaminated air entered the air duct on the left it passed by the UV lamps and through the catalyst filter where it was treated. The treated air then traveled down the air duct and exited on the right where it re-entered the room and was mixed back in with the contaminated air.

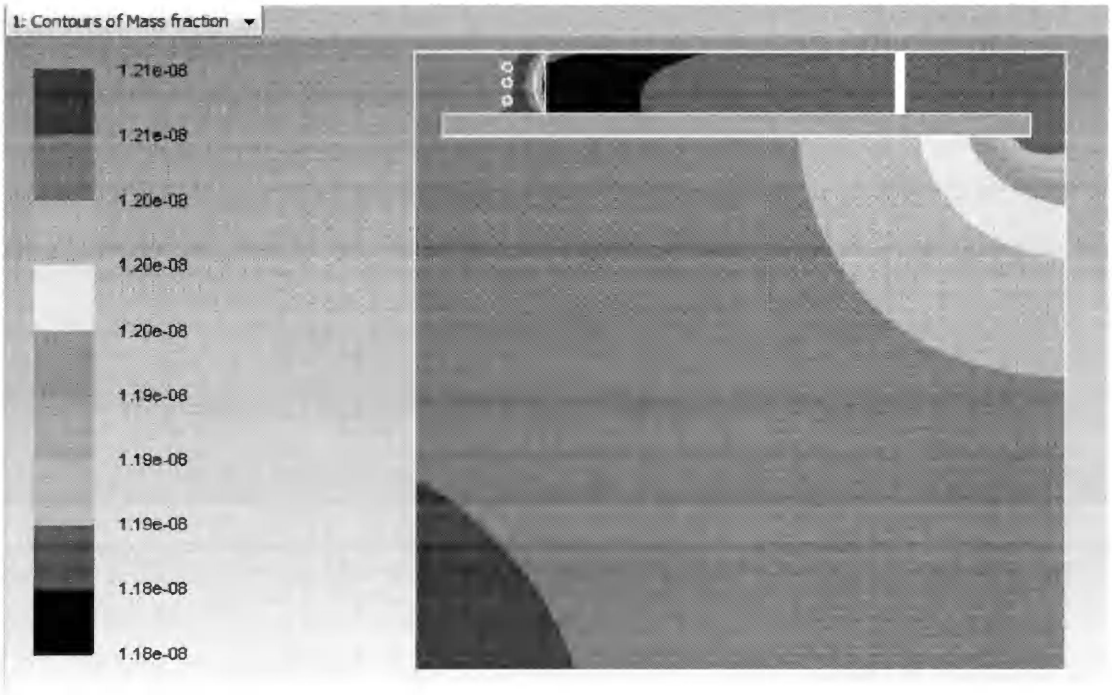

Figure 25: Concentration profile of butyric acid throughout the closed room after 4.5 hours

Similar to the first case, it appears that the closed system is behaving as a batch reactor. That means that the hydrodynamics of the air through the room should be well known and easily modeled with CFD software.

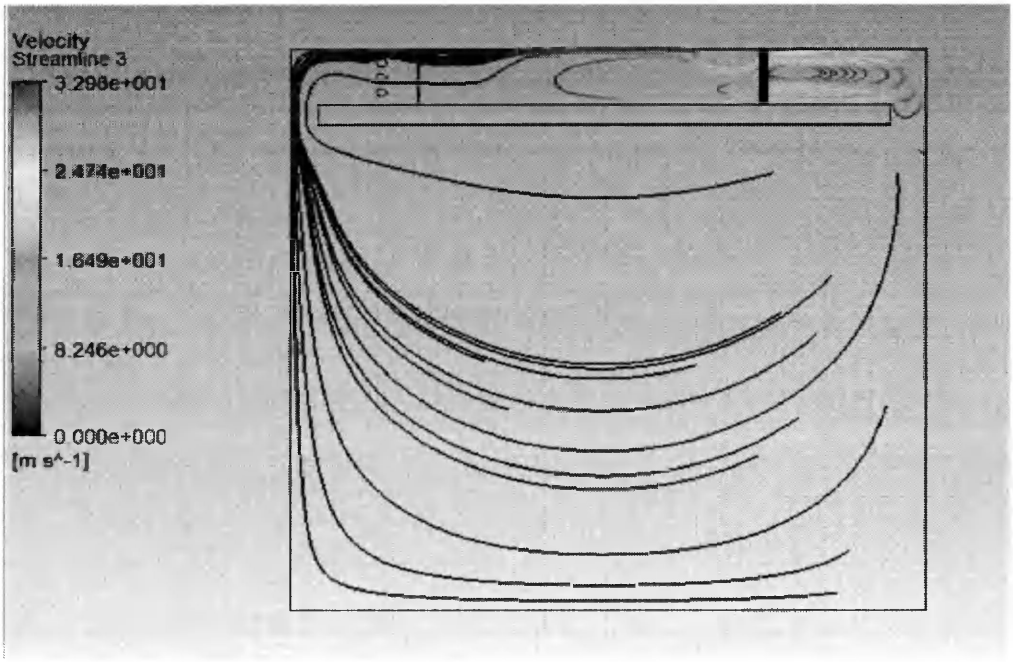

Figure 26: Streamline path of air through system

A major concern when running the PCO system within a home would be human exposure to the UV radiation. As shown in Figure 27, in this case study all of the UV radiation is contained within the air duct system and is not entering the room. This setup would be ideal for any applications where there is the potential for human contact since it eliminates any potential exposure to the harmful UV radiation. By using a full scale CFD model we can determine if there are not only hydrodynamic or mass transfer issues that need to be addressed, but also if there are any issues with the radiation field. Looking at Figure 27, it appears that the UV irradiance level across the catalyst filter might not be uniform. The UV irradiance level will be higher at the center of the filter than at the two ends, similar to the second case. This could be fixed by adjusting the location of the UV lamps with respect to the catalyst filter.

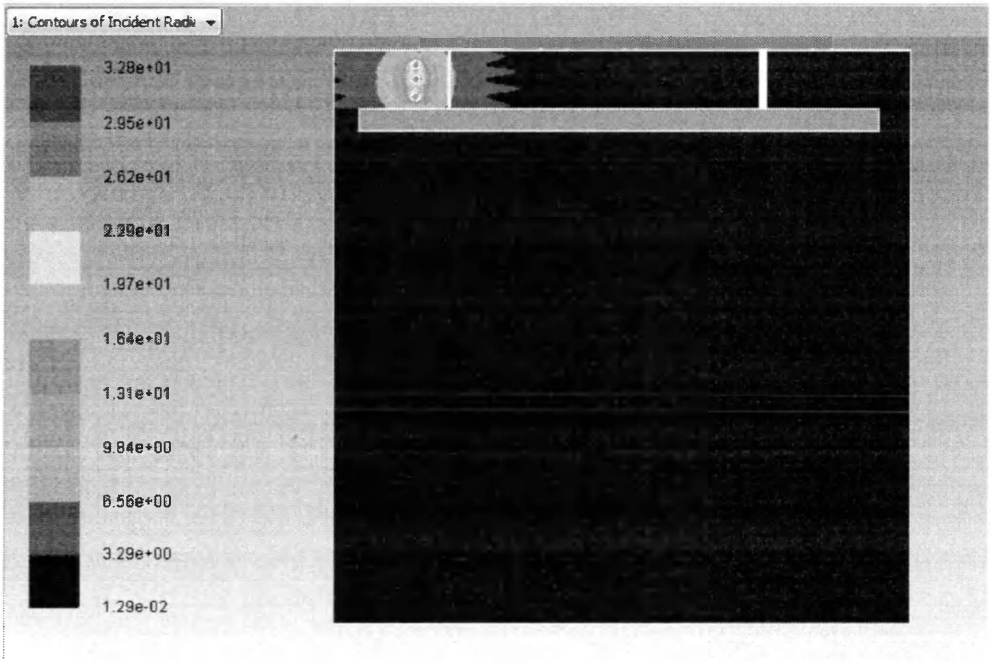

Figure 27: Radiation field throughout system

From Figure 28 it is seen that with an initial butyric acid concentration of around 1 ppmv the system took approximately 4 hours to reach a steady state at a final butyric acid concentration of 11.3 ppbv, which is below the odor threshold for butyric acid 240 ppbv(Leffingwell & Associates, 2008). Since butyric acid has a very rancid smell anything above the odor threshold would be uncomfortable. With a final butyric acid concentration well below the odor threshold the system was capable of returning the room to a comfortable level.

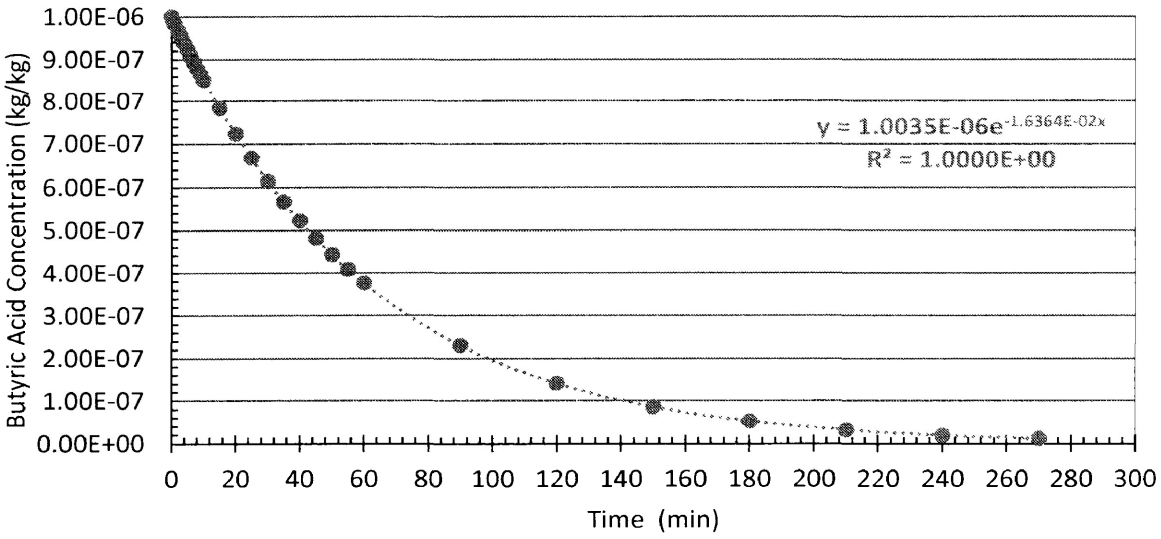

Figure 28: Model results without butyric acid source

4.3.2 PCO System with Point Source

When the constant butyric acid source was introduced the overall removal rate of butyric acid did decreased, which can be expected. After 4 hours the butyric acid concentration dropped to 23.6 ppbv, which is again below the odor threshold for butyric acid. This demonstrates that in this case the PCO system was capable of treating the contaminated air as well as handling the constant emission of butyric acid. In fact, after about an hour and a half (88 min) the butyric acid in the room had already dropped to just below the odor threshold.

When the model ran a third time, this time in the case of two people standing in the room, the same trend was seen. After 4 hours the concentration of butyric acid in the room had dropped to 32.1 ppbv. Again the system was capable of treating the contaminated air and handling the constant emission of butyric acid. In the case of two people in the closed room the system required a little over an hour and a half (94 min) to reduce the butyric acid concentration below the odor threshold.

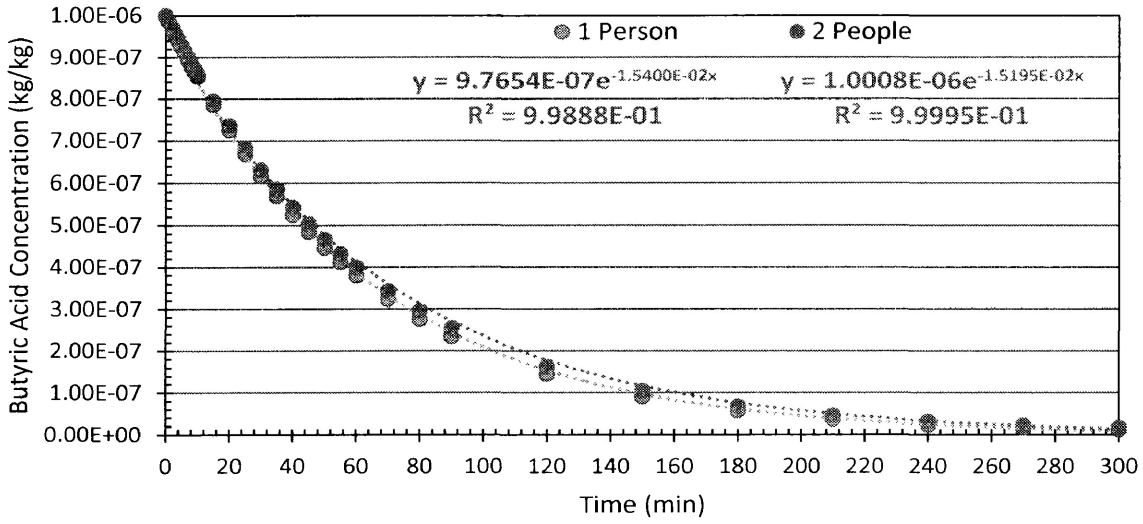

Figure 29: Model results with a constant source of butyric acid

4.3.3 Evaluating System Performance

From these results, the performance of the PCO system could be optimized by evaluating the UV irradiance levels on the catalyst surface as well as the hydrodynamics within the system. Using CFD, different distances between the UV lamps and the catalyst surface could be modeled in order to determine the optimal distance for this configuration. Also, different UV irradiance levels could be tested to determine the most energy efficient UV irradiance level for this system. This step was not taken due to time constraints, but this simple case model could be used as the basis for a new thesis project using CFD to model full scale PCO treatment systems for various applications.

In order to simplify this case study, only one room with a closed duct system was modeled. However, CFD could also be used to model an entire home or office building with multiple rooms and duct lines in 3D at full scale. A full scale model of a home or office building can also be used to determine how the PCO system will perform under varying air flow rates since the flow rate of air throughout an air duct system will vary at different points along the duct line. The flow rate will also vary as heating and air conditioning systems are turned on and off. This full scale model would allow the user to obtain a more accurate portrayal of how VOC levels would be changing within the different rooms of a home or office building as the air is recirculated throughout the entire structure.

4.4 Conclusions

This case study demonstrates how the new proposed approach to reaction modeling developed in this thesis could be used to predict PCO system performance treating air in a home. In this case, the PCO system was capable of treating air contaminated with butyric acid and was able to quickly reduce the concentration below the odor threshold. The system was capable of treating the air when constant sources of butyric acid were present.

By developing a rate of reaction that describes only what is happening at the catalyst surface, the rate of reaction is no longer dependent on the overall system geometry and operating conditions. By using CFD to model the PCO system within a home or office building researchers can determine if the system is capable of treating the contaminants present and to what degree it can remove the VOCs without having to install and monitor a system.

Chapter 5 – Conclusions and Future Work

A new approach was developed to adjust experimental reaction rate expressions for PCO systems in order to reflect the actual rate of reaction happening on a catalyst surface. This approach considered the reacting volume as happening only within a thin layer of cells just above the reactive catalyst surface. Through a series of steps, the reaction rate expressions became dependent solely on the concentration of air contaminants, e.g. formaldehyde, at the surface, as opposed to the bulk concentrations. This meant that the change in concentration that is being calculated using on the surface of the catalyst, unlike the experimental reaction rates, which are based on the bulk concentrations that are dependent on both reaction kinetics and mass transfer effects. Two case studies were used to demonstrate how this new approach can be employed to adapt the experimental reaction rates in order to reflect the actual rate of reaction on the catalyst surface.

In the first case, the experimental kinetic model for formaldehyde decomposition (simple case) was adapted to reflect surface reactions based on VOC levels on the catalyst surface. Using the developed approach to adapt the experimental reaction rates a new reaction rate model was developed that was able to accurately predict the rate of formaldehyde decomposition over time. The results from this first case study showed that the new reaction rate model was independent of mass transfer effects within the system. A complete CFD model was developed for the system considering hydrodynamics, species transport, and reaction kinetics, and it was in agreement with the experimental data that was reported by the author. The complete CFD model showed how CFD can be used to optimize system design by calculating the flow path of the air through the system and the concentration profile of the target VOC within the system. In this case the complete CFD model showed that the closed system was behaving like a perfect mixed batch reactor and a uniform concentration profile throughout the bulk of the system.

Prior to introducing the reaction rates into the CFD model the reaction rate expressions were tested in Microsoft Excel software in order to determine if the rate expressions would predict concentrations within an acceptable range of the experimental results when considering kinetics alone. As seen in the second case, complete CFD models were still required in order to account for any other influencing factors, such as mass transfer limitations and variations in the UV

irradiance levels that would impact the overall rate of decomposition of the target VOC. In the second case, after examining the complete CFD model it became apparent that there were hydrodynamic issues within the reactor that would cause mass transfer limitation within the system. In real life, these limitations could result in a drop in reactor performance and a shorter life span of the catalyst if this reactor configuration was run at full scale. At the end, the rate model was able to predict the rate of decomposition for butyric acid in the air for a variety of initial concentrations and UV irradiance levels at the catalyst surface. In this case, the CFD model results also disproved the general assumption that UV irradiance levels are uniform across the catalyst surface. After examining the UV irradiance levels across the catalyst surface, it was determined that the irradiance level drops significantly across the catalyst surface from the center to the outside edges.

A simple case study was also developed in order to demonstrate how the proposed approach to reaction modeling could be used to predict PCO system performance treating air in a home. In this case, the PCO system was tasked with treating air contaminated with butyric acid and was able to quickly reduce the concentration below the odor threshold. This simple case study proves the strong capability of CFD modeling to model full scale applications of a PCO when integrated into an existing air duct system. In this case, only a single study room with a closed air duct system was modeled. However, it demonstrates how CFD can also be used to predict the performance of the PCO system in treating contaminated air throughout an entire home.

Future Work

Due to time limitations, the case study performed in this research was very basic in order to demonstrate the potential applications of this research. The next step in this research would be to perform a full scale case study to determine how the PCO system would perform under different operating conditions for treating VOCs within a home. The full scale case study should consider:

1. A full-scale home with multiple rooms (each of which could contain different levels of VOCs or different target pollutants) and a complete HVAC system;
2. Varying hydrodynamics due different HVAC conditions for heating, cooling, and circulation;

3. The home as both a batch reactor (closed system with no fresh air entering the home or exhaust air leaving the home) and a CSTR reactor (open system with some fresh air being supplied to the home from outside and some air being exhausted from the home);
4. Optimization of the PCO reactor within the air duct (reactor location, lamp location, UV intensity);
5. The maximum load the PCO system could handle with different VOC sources throughout the home.

References

Alberici, R. M., & Jardim, W. F. (1997). Photocatalytic destruction of VOCs in the gas-phase using titanium dioxide. *Applied Catalyst B: Environmental , 14*, 55-68.

Ao, C., & Lee, S. (2004). Combination effect of activated carbon with TiO2 for hte photodegradation of binary pollutants at typical indoor air levels. *Journal of Photochemistry and Photobiology A: Chemistry , 161*, 131-140.

Assadi, A. A., Bouzaza, A., & Wolbert, D. (2012). Potocatalytic oxidation of trimethylamine and isovaleraldehyde in an annular reactor: Influence of the mass transfer and the relative humidity. *Journal of Photochemistry and Photobiology A: Chemistry , 236*, 61-69.

Assadi, A. A., Palau, J., Bouzaza, A., & Wolbert, D. (2013). Modeling of a continuous photocatalytic reactoer for isovaleraldehyde oxidation: Effects of different operating parameters and chemical degradation pathway. *Chemical Engineering Research and Design , 91*, 1307-1316.

Brosillon, S., Llomme, L., Vallet, C., Bouzaza, A., & Wolbert, D. (2008). Gas phase photocatalysis and liquid phase photocatalysis: Interdependence and influence of substrate concentration and photon flow on degradation reaction rates. *Applied Catalysis B: Environmental , 78*, 232-241.

Canadian Lung Association. (2012, September). *The Lung Association: Pollution and Air Quality.* Retrieved November 2013, from The Lung Association: http://www.lung.ca/protect-protegez/pollution-pollution/indoor-interieur/home-chezvous_e.php#dry

Charles, G., Roques-Carmes, T., Nidhal, B., Falk, L., Commenge, J.-M., & Corbel, S. (2011). Determination of kinetic constants of a photocatalytic reaction in micro-channel reactors in the presence of mass-transfer limitation and axial dispersion. *Journal of Photochemistry and Photobiology A: Chemistry , 223*, 202-211.

Chong, S., Wang, S., Tade, M., Ang, H. M., & Pareek, V. (2011). Simulations of photodegradation of toluene and formaldehyde in a monolith reactor using computational fluid dynamics. *AlChE Journal , 57*, 724-734.

Cooper, C. D., & Alley, F. C. (2011). *Air Pollution Control A Design Approach* (4th ed.). Long Grove, IL, United States: Waveland Press, Inc.

Cybulski, A., & Moulijn, J. A. (2006). Treatment of VOC Emissions from Stationary Sources. In *Structured Catalysts and Reactors* (pp. 147-170). Boca Raton: CRC Press.

Destaillats, H., Sleiman, M., Sullivan, D. P., Jacquiod, C., & Sablayrolles, J. (2012). Key parameters influencing the performance of photocatalytic oxidation (PCO) air purification under realistic indoor conditions. *Applied Catalysis B: Environmental , 128*, 159-170.

Deveau, P.-A., Arsac, F., Thivel, P.-X., Ferronato, C., Delpeh, F., Choven, J.-M., et al. (2007). Different methods in TiO2 photodegradation mechanism studies: Gaseous and TiO2-adsorbed phases. *Journal of Hazardous Materials , 144*, 629-697.

Duran, J. E., Mohseni, M., & Taghipour, F. (2010). Modeling of annular reactors with surface reaction using computational fluid dynamics (CFD). *Chemical Engineerign , 65*, 1201-1211.

Hodgson, A. T., Beal, D., & McIlvaine, J. E. (2002). Sources of formaldehyde, other aldehydes and terpenes in a new manufactured house. *Indoor Air , 12*, 235-242.

Hodgson, A. T., Destaillats, H., Sullivan, D. P., & Fisk, W. J. (2007). Performance of ultraviolet photocatalytic oxidation for indoor air cleaning applications. *Indoor Air , 17*, 305-316.

Hossain, M., Raupp, G., Hay, S., & Obee, T. (1999). Three-dimensional developing flow model for photocatalytic monolith reactors. *AlChE Journal , 45*, 1309-1321.

Huang, Q., Liu, T., Yang, J., Yao, L., & Gao, L. (2011). Evaluation of radiative transfer using the finite volume method in cylindrical photoreactors. *Chemical Engineering Science , 66*, 3930-3940.

Imoberdorf, G. E., Irazoqui, H. A., Alfano, O. M., & Cassano, A. E. (2007). Scaling-up from first principles of a photocatalytic reactor for air pollution remediation. *Chemical Engineering Science , 62*, 793-804.

Imoberdorf, G. E., Taghipour, F., & Mohseni, M. (2008). Radiation field modeling of multi-lamp, homogeneous photoreactors. *Journal of Photochemistry and Photobiology A: Chemistry , 198*, 169-178.

Jovic, F., Kosar, V., Tomasic, V., & Gomzi, Z. (2012). Non-ideal flow in an annular photocatalytic reactor. *Chemical Engineering Research and Design , 90*, 1297-1306.

Kabir, E., & Kim, K.-H. (2011). An investigation on hazardous and odorous pollutant emissions during cooking activities. *Journal of Hazardous Materials , 188*, 443-454.

Kagi, N., Tamura, H., & Namiki, N. (2009). Secondary VOC emissions from flooring material surfaces exposed to ozone or UV irradiation. *Building and Environment* , 129-138.

Keller, V., Bernhardt, P., & Garin, F. (2003). Photocatlytic oxidation of butyl acetate in vapor phase on TiO2, Pt/TiO2 and WO3/TiO2 catalysts. *Journal of Catalysis , 215*, 129 - 138.

Kumar, J., & Bansal, A. (2012). CFD modeling of hydrodynamics and mass transfer of Rhodamine B in annular reactor. *Heat Mass Transfer , 48*, 2069-2077.

Launder, B., & Spalding, D. (1974). The numerical computation of turbulent flows. *Computer Methods in Applied Mechanics and Engineering , 3* (2), 269-289.

Lee, D. M., Yun, H. J., Yu, S., Yun, S. J., Lee, S. Y., Kang, S. H., et al. (2012). Design of an efficient photocatalytic reactor for the decomposition of gaseous organic contaminants in air. *Chemical Engineering Journal , 187*, 203-209.

Leffingwell & Associates. (2008). *Odor Thresholds.* Retrieved April 2, 2014, from Leffingwell & Associates: http://www.leffingwell.com/odorthre.htm

Lin, L., Chai, Y., Zhao, B., Wei, W., He, D., He, B., et al. (2013). Photocatalytic oxidation for degradation of VOCs. *Open Journal of Inorganic Chemistry , 3*, 14-25.

Liu, M. S., & Peng, M. (2005). Verification of mass transfer simulation with CFD using highly accurate solutions. *Computers and electronics in agriculture , 49*, 309-314.

Lopes, F. V., Monteiro, R. A., Silva, A. M., Silva, G. V., Faria, J. L., Mendes, A. M., et al. (2012). Insights into UV-TiO2 photocatalytic degradation of PCE for air decontamination systems. *Chemical Engineering Journal , 204-206*, 244-257.

Mo, J., Zhang, Y., Xu, Q., Lamson, J. J., & Zhao, R. (2009). Photocatalytic purification of volative organic compounds in indoor air: A literature review. *Atmospheric Environment , 43*, 2229-2246.

Obee, T. N., & Brown, R. T. (1995). TiO2 photocatalysis for indoor air applications: Effects of humidity and trace contaminant levels on the oxidation rates of formaldehyde, toluewne, and 1,3-butadiene. *Envrionmental Science and Technology , 29*, 1223-1231.

Ohko, Y., Fujishima, A., & Hashimoto, K. (1998). Kinetic analysis of the photocatalytic degradation of gas-phase 2-propanol under mass transport-limited conditions with a TiO2 film photocatalyst. *Journal of Physical Chemistry B: , 102*, 1724-1729.

Pareek, V., Cox, S., Brungs, M., Young, B., & Adesina, A. (2003). Computational Fluid Dynamics (CFD) simulation of a pilot-scale annular bubble column photocatalytic reactor. *Chemical Engineering Science , 58*, 859-865.

Passalia, C., Alfano, O. M., & Brandi, R. J. (2012). A methodology for modeling photocatalytic reactors for indoor pollution control using previously estimated kinetic parameters. *Journal of Hazardous Materials , 211-212*, 357 - 365.

Pichat, P. (2010). Some views about indoor air photocatalytic treatment using TiO2: Conceptualization of humidity effects, active oxygen species, problem C1-C4 carbonyl pollutants. *Applied Catalysis B: Environmental , 99*, 428-434.

Queffeulou, A., Geron, L., & Shaer, E. (2012). Prediction of photocatalytic air purifier apparatus performances with a CFD approach using experimentally determined kinetic parameters. *Chemical Engineering Science , 65*, 5067 - 5074.

Queffeulou, A., Geron, L., Archambeau, C., Le Gall, H., Marquaire, P.-M., & Zahraa, O. (2010). Kinetic study of acetaldehyde photocatalytic oxidation with a thin film of TiO2 coated on stainless steel and CFD modeling approach. *Industrial and Engineering Chemistry Research , 49*, 6890-6897.

Quiceno, R., Perez-Ramirez, J., Warnatz, J., & Deutschemann, O. (2006). Modeling the high-temperature catalytic partial oxidation of methane over platinum gauze: Detailed gas-phase and

surface chemistries coupled with 3D flow field simulations. *Applied Catalysis A: General , 303*, 166-176.

Raupp, G. B., Alexiadis, A., Hossain, M. M., & Changrani, R. (2001). First-principles modeling, scaling laws and design of structured photocatalytic oxidation reactor for air purification. *Catalysis Today , 69*, 41-49.

Sakamoto, T., Doi, S., & Torii, S. (1999). Effects of formaldehyde, as an indoor air pollutant, on the airway. *Allergology International , 48*, 151-160.

Salonen, H., Pasanen, A.-L., Lappalainen, S., Riuttala, H., Tuomi, T., Pasanen, P., et al. (2009). Volatile Organic Compounds and Formaldehyde as explaining factors for sensory irritation in office environments. *Journal of Occupational and Environmental Hygiene , 6*, 239-247.

Salvado-Estivill, I., Hargreaves, D. M., & Puma, G. L. (2007). Evaluation of the intrinsic photocatalytic oxidation kinetics of indoor air pollutants. *Envrionmental Science and Technology , 41*, 2028-2035.

Shie, J.-L., Lee, C.-H., Chiou, C.-S., Chang, C.-T., Chang, C.-C., & Chang, C.-Y. (2008). Photodegradation kinetics of formaldehyde using light sources of UVA, UVC and UVLED in the presence of composed silver titanium oxide photocatalyst. *Journal of Hazardous Materials , 155*, 164 - 172.

Shin, S. H., & Jo, W. K. (2012). Volatile organic compound concentations, emission rates, and source apportionment in newly-built aparements at pre-occupancy stage. *Chemosphere* , 569-578.

Shiraishi, F., Ikeda, S., & Kamikariya, N. (2009). Photocatalytic decompositions of gaseous HCHO over thin films of anatase titanium oxide converted from amorphous in a heated air and in an aqueous solution of hydrogen peroxide. *Chemical Engineering Journal , 148*, 234-241.

Shiraishi, F., Ohkubo, D., Toyoda, K., & Yamaguchi, S. (2005a). Decomposition of gaseous formaldehyde in a photocatalytic reactor with a parallel array of light sources 1. Fundamental experiment for reactor design. *Chemical Engineering Journal , 114*, 153 - 159.

Shiraishi, F., Toyoda, K., & Miyakawa, H. (2005b). Decomposition of gaseous formaldehyde in a photocatalytic reactor with a parallel array of light sources 2. Reactor preformance. *Chemical Engineering Journal , 114*, 145-151.

Singh, M., Salvado-Estivill, I., & Li Puma, G. (2007). Radiation field optimization in photocatalytic monolith reactors for air treatment. *AIChE , 53.*, 678-686.

Sozzi, D., & Taghipour, F. (2006). UV reactor performance modeling by eulerian and lagrangian methods. *Envrionmental Science and Technology , 40*, 1609-1615.

Taranto, J., Frochot, D., & Pichat, P. (2007). Modeling and optimizing irradiance on planar, folded, and honeycomb shapes to maximize photocatalytic air purification. *Catalysis Today , 122*, 66-77.

Taranto, J., Frochot, D., & Pichat, P. (2009). Photocatalytic air purification: Comparative efficacy and pressure drop of a TiO2-coated thin mesh and a honeycomb monolith at high air velocities using a 0.4 m3 close-loop reactor. *Separation and Purification Technology , 67*, 187-193.

The Engineering Toolbox. (2014). *Rectangular Duct Sizes*. Retrieved March 2014, from The Engineering Toolbox.

Treybal, R. E. (1980). Molecular Diffusion in Fluids. In J. J. Carberry, J. R. Fair, W. R. Schowalter, & J. Wel (Eds.), *Mass-Transfer Operations* (pp. 21-44). New York: McGraw-Hill.

Wang, K.-H., Hsieh, Y.-H., & Hsieh, Y.-H. (1998). A study of photocatalytic degradation of trichloroethylene in vapor phase on TiO2 photocatalyst. *Chemospere , 36*, 2763-2773.

Wang, Z., Liu, J., Dai, Y., Dong, W., Zhang, S., & Chen, J. (2012). CFD modeling of a UV-LED photocatalytic odor abatement process in a continuous reactor. *Journal of Hazardous Materials , 215-216*, 25-31.

Yang, R., Zhang, Y.-P., & Zhao, R.-Y. (2004). An improved model for analyzing the performance of photocatalytic oxidation reactors in removing volatile organic compounds and its application. *Journal of the Air & Waste Management Association , 54*, 1516-1524.

Zhang, T., Wei, C., Feng, C., & Zhu, J. (2012). A novel airlift reactor enhanced by funnel internals and hydrodynamics prediction by the FCD method. *Bioresource Technology , 104*, 600 - 607.

Zhao, J., & Yang, X. (2003). Photocatalytic oxidation for indoor air purification: a literature review. *Building and Environment , 38*, 645-654.

Zhong, L., Haghighat, F., & Lee, C.-S. (2013). Ultraviolet photocatalytic oxidation for indoor environment applications: Experimental validation of the model. *Building and Environment , 62*, 155-166.

Zhong, L., Haghighat, F., Blondeau, P., & Kozinski, J. (2010). Modeling and physical interpretation of photocatalytic oxidation efficiency in indoor air applications. *Building and Environment , 45*, 2689-2697.

Appendix A: UDF Sources Codes - First Case

First Approach

```
/************************************************************************

Custom surface reaction rate UDF

************************************************************************/

#include "udf.h"

#include "mem.h"


#define K1 0.001995


DEFINE_INIT(RESET,d)

{

        Thread *t;

        cell_t c;

        face_t f;

        real A[ND_ND], area, t_ID, vol;

        // Loop over all threads in the domain and reset the memory to zero

        thread_loop_c(t,d)

        {

                begin_c_loop(c,t)

                {
```

```
            C_UDMI(c,t,0)=0;
        }
        end_c_loop(c,t)
    }
```

// Loop over face on specified wall to reset the UDM of adjacent cell to Volume of Cell/ Area of Face

```
    thread_loop_f(t,d)
    {
        t_ID=THREAD_ID(t);
        //For this case the reaction is happening on the surface with ID=7
        if (t_ID==9)
        {
            begin_f_loop (f,t)
            {
                // Calculate the area of the face
                F_AREA(A,f,t);
                area=NV_MAG(A);
                // Calculate the volume of adjacent cell
                vol=C_VOLUME(F_C0(f,t),THREAD_T0(t));
                C_UDMI(F_C0(f,t),THREAD_T0(t),0)=area/vol;
            }
```

```
                end_f_loop(f,t)
            }
        }
        printf("all memories are reset to zero, cell on the specified wall isreset to %f\n",
vol/area);
}

DEFINE_SOURCE(CH2O_source, c, t, dS, eqn)
{
        real source, C_ch2o, rate1;
        C_ch2o=C_YI(c,t,0);
        rate1=K1*C_ch2o*C_R(c,t)/30;
        C_UDMI(c,t,1)=rate1;
        return C_UDMI(c,t,0)*C_UDMI(c,t,1)*(-30);
        //return source;
}

DEFINE_SOURCE(O2_source, c, t, dS, eqn)
{
        real source;
        return C_UDMI(c,t,0)*C_UDMI(c,t,1)*(-32);
```

```
        //return source;
}

DEFINE_SOURCE(CO2_source, c, t, dS, eqn)
{
        real source;
        return C_UDMI(c,t,0)*C_UDMI(c,t,1)*44;
        //return source;
}

DEFINE_SOURCE(H2O_source, c, t, dS, eqn)
{
        real source;
        return C_UDMI(c,t,0)*C_UDMI(c,t,1)*18;
        //return source;
}
```

Second Approach

```
/************************************************************************

Custom surface reaction rate UDF

************************************************************************/

#include "udf.h"

#include "mem.h"


#define K1 0.001007

#define K2 0.012171166


DEFINE_INIT(RESET,d)

{

        Thread *t;

        cell_t c;

        face_t f;

        real A[ND_ND], area, t_ID, vol;

        // Loop over all threads in the domain and reset the memory to zero

        thread_loop_c(t,d)

        {

                begin_c_loop(c,t)

                {
```

```
            C_UDMI(c,t,0)=0;
        }
        end_c_loop(c,t)
    }
    // Loop over face on specified wall to reset the UDM of adjacent cell to Volume of Cell/
Area of Face
    thread_loop_f(t,d)
    {
        t_ID=THREAD_ID(t);
        //For this case the reaction is happening on the surface with ID=7
        if (t_ID==9)
        {
            begin_f_loop (f,t)
            {
                // Calculate the area of the face0.00
                 F_AREA(A,f,t);
                area=NV_MAG(A);
                // Calculate the volume of adjacent cell
                vol=C_VOLUME(F_C0(f,t),THREAD_T0(t));
                C_UDMI(F_C0(f,t),THREAD_T0(t),0)=area/vol;
            }
```

```
                end_f_loop(f,t)
            }
        }
        printf("all memories are reset to zero, cell on the specified wall isreset to %f\n",
vol/area);
}

DEFINE_SOURCE(CH2O_source, c, t, dS, eqn)
{
        real source, C_ch2o, rate1;
        C_ch2o=C_YI(c,t,0);
        rate1=K1/(1+K1/K2)/30*C_R(c,t)*C_ch2o;
        C_UDMI(c,t,1)=rate1;
        source=-C_UDMI(c,t,0)*30*rate1;
        return source;
}

DEFINE_SOURCE(O2_source, c, t, dS, eqn)
{
        real source;
        //C_ch2o=C_YI(c,t,0);
```

```
        //rate1=C_ch2o*K1/(1+K2);
        source=C_UDMI(c,t,0)*-C_UDMI(c,t,1)*32;
        return source;
}

DEFINE_SOURCE(CO2_source, c, t, dS, eqn)
{
        real source;
        //C_ch2o=C_YI(c,t,0);
        //rate1=C_R(c,t)*C_ch2o*29/30*K1/(1+K2);
        source=C_UDMI(c,t,0)*C_UDMI(c,t,1)*44;
        return source;
}

DEFINE_SOURCE(H2O_source, c, t, dS, eqn)
{
        real source;
        //C_ch2o=C_YI(c,t,0);
        //rate1=C_R(c,t)*C_ch2o*29/30*K1/(1+K2);
        source=C_UDMI(c,t,0)*C_UDMI(c,t,1)*18;
        return source;
```

```
}
```

Thirst Approach

```
/************************************************************************

Custom surface reaction rate UDF

************************************************************************/

#include "udf.h"

#include "mem.h"


DEFINE_INIT(RESET,d)

{

        Thread *t;

        cell_t c;

        face_t f;

        real A[ND_ND], area, t_ID, vol;

        //Loop over all threads in the domain and reset the memory to zero

        thread_loop_c(t,d)

        {

                begin_c_loop(c,t)

                {

                        C_UDMI(c,t,0)=0;

                }

                end_c_loop(c,t)
```

```
}
// Loop over face on specified wall to reset the UDM of adjacent cell to Volume of Cell/
Area of Face
thread_loop_f(t,d)
{
        t_ID=THREAD_ID(t);
        //For this case the reaction is happening on the surface with ID=7
        if (t_ID==9)
        {
                begin_f_loop (f,t)
                {
                        // Calculate the area of the face0.00
                        F_AREA(A,f,t);
                        area=NV_MAG(A);
                        // Calculate the volume of adjacent cell
                        vol=C_VOLUME(F_C0(f,t),THREAD_T0(t));
                        C_UDMI(F_C0(f,t),THREAD_T0(t),0)=1;
                }
                end_f_loop(f,t)
        }
}
```

```
        printf("all memories are reset to zero, cell on the specified wall isreset to %f\n", 1/vol);
}


DEFINE_SOURCE(CH2O_source, c, t, dS, eqn)
{
        real source,C_ch2o, rate1;
        //C_ch2o = kg/m3 ch2o
        C_ch2o=C_YI(c,t,0)*C_R(c,t);
        // rate = kg/m3/s
        if (C_ch2o>=0.000000765432)
        {
                rate1=((-1.932e3)*pow(C_ch2o,2.)+(3.677e-3)*C_ch2o-(1.59e-9))*1100;
        }
        else if (C_ch2o<0.000000765432)
        {
                rate1=((3.685e23)*pow(C_ch2o,5.)-
(9.897e17)*pow(C_ch2o,4.)+(1.044e12)*pow(C_ch2o,3.)-
(5.413e5)*pow(C_ch2o,2.)+(0.1383)*C_ch2o-(1.393e-8));
        }

        C_UDMI(c,t,1)=rate1*3806;
        source=C_UDMI(c,t,0)*(-rate1);
```

```
        //source=rate1;
        return source;
}

DEFINE_SOURCE(O2_source, c, t, dS, eqn)
{
        real source;
        //C_ch2o=C_YI(c,t,0);
        //rate1=C_ch2o*K1/(1+K2);
        source=C_UDMI(c,t,0)*C_UDMI(c,t,1)*(-32/30);
        return source;
}

DEFINE_SOURCE(CO2_source, c, t, dS, eqn)
{
        real source;
        //C_ch2o=C_YI(c,t,0);
        //rate1=C_R(c,t)*C_ch2o*29/30*K1/(1+K2);
        source=C_UDMI(c,t,0)*C_UDMI(c,t,1)*(44/30);
        return source;
}
```

```
DEFINE_SOURCE(H2O_source, c, t, dS, eqn)
{
        real source;
        //C_ch2o=C_YI(c,t,0);
        //rate1=C_R(c,t)*C_ch2o*29/30*K1/(1+K2);
        source=C_UDMI(c,t,0)*C_UDMI(c,t,1)*(18/30);
        return source;
}
```

Appendix B: UDF Sources Codes – Second Case

```
/************************************************************************

Custom surface reaction rate UDF

************************************************************************/

#include "udf.h"

#include "mem.h"

#include "sg_disco.h"


#define a 9.44314e-11//rate constants based on Co 195 and 384 mg/m3 with Io=0

#define b 0.31818

#define e 0.004160567

#define C_DO(c,t)C_STORAGE_R_XV(c,t,SV_DO_IRRAD,0)


DEFINE_INIT(RESET,d)

{

        Thread *t;

        cell_t c;

        face_t f;

        real A[ND_ND], area, t_ID, vol;
```

```
// Loop over all threads in the domain and reset the memory to zero
thread_loop_c(t,d)
{
        begin_c_loop(c,t)
        {
                C_UDMI(c,t,0)=0;
        }
        end_c_loop(c,t)
}
// Loop over face on specified wall to reset the UDM of adjacent cell to Volume of Cell/
Area of Face
thread_loop_f(t,d)
{
        t_ID=THREAD_ID(t);

        if (t_ID==23) //catalyst wall ID.  Must use a new if statement for each thread ID
        {
                begin_f_loop (f,t)
                {
                        // Calculate the area of the face0.00
                        F_AREA(A,f,t);
```

```
                area=NV_MAG(A);
                // Calculate the volume of adjacent cell
                vol=C_VOLUME(F_C0(f,t),THREAD_T0(t));
                C_UDMI(F_C0(f,t),THREAD_T0(t),0)=area/vol;
            }
            end_f_loop(f,t)
        }
        else if (t_ID==30) //filter surface ID
        {
            begin_f_loop (f,t);
            {
                // Calculate the area of the face0.00
                F_AREA(A,f,t);
                area=NV_MAG(A);
                // Calculate the volume of adjacent cell
                vol=C_VOLUME(F_C0(f,t),THREAD_T0(t));
                C_UDMI(F_C0(f,t),THREAD_T0(t),0)=area/vol;
            }
            end_f_loop(f,t)
        }
}
```

```
        printf("all memories are reset to zero, cell on the specified wall isreset to %f\n",
vol/area);
}
DEFINE_SOURCE(BUTYRIC_source, c, t, dS, eqn)
{
        real source;
        real C_butyric, rate1, Irrad;
        C_butyric=C_YI(c,t,0)*C_R(c,t)*10e6; //C in mg/m3
        Irrad=C_DO(c,t); //I in W/m2 (Adjusting as I on catalyst surface changes)
        rate1=(a*Irrad/(1+b*Irrad+e*C_butyric)*C_butyric);  //rate in kmol/m3-system/s
        C_UDMI(c,t,1)=(0.0216/0.361)*C_UDMI(c,t,0)*rate1*0.5;  //rate in kmol/m3-cell/s
        C_UDMI(c,t,2)=Irrad;
        source=-C_UDMI(c,t,1)*88.11; //source in kg/m3/s
        //source=C_ch2o*(-rate1);
        return source;
}

DEFINE_SOURCE(O2_source, c, t, dS, eqn)
{
        real source;
        //C_ch2o=C_YI(c,t,0);
```

```
        //rate1=C_ch2o*K1/(1+K2);
        source=C_UDMI(c,t,1)*32*-5;
        return source;
}

DEFINE_SOURCE(CO2_source, c, t, dS, eqn)
{
        real source;
        //C_ch2o=C_YI(c,t,0);
        //rate1=C_R(c,t)*C_ch2o*29/30*K1/(1+K2);
        source=4*C_UDMI(c,t,1)*44;
        return source;
}

DEFINE_SOURCE(H2O_source, c, t, dS, eqn)
{
        real source;
        //C_ch2o=C_YI(c,t,0);
        //rate1=C_R(c,t)*C_ch2o*29/30*K1/(1+K2);
        source=4*C_UDMI(c,t,1)*18;
        return source;
```

```
}


DEFINE_PROPERTY(Absorption_coefficient,c,t)
{
        real abs_coeff;


        abs_coeff=41.77*C_YI(c,t,0)+3e-17;
}
```

Appendix C: UDF Sources Codes – Case Study

```
/************************************************************************

Custom surface reaction rate UDF

************************************************************************/

#include "udf.h"

#include "mem.h"

#include "sg_disco.h"


#define a 9.44314e-11//rate constants based on Co 195 and 384 mg/m3 with Io=0

#define b 0.31818

#define e 0.004160567

#define C_DO(c,t)C_STORAGE_R_XV(c,t,SV_DO_IRRAD,0)


DEFINE_INIT(RESET,d)

{

        Thread *t;

        cell_t c;

        face_t f;

        real A[ND_ND], area, t_ID, vol;
```

```
// Loop over all threads in the domain and reset the memory to zero
thread_loop_c(t,d)
{
        begin_c_loop(c,t)
        {
                C_UDMI(c,t,0)=0;
        }
        end_c_loop(c,t)
}
// Loop over face on specified wall to reset the UDM of adjacent cell to Volume of Cell/
Area of Face
thread_loop_f(t,d)
{
        t_ID=THREAD_ID(t);

        if (t_ID==13) //catalyst wall ID.  Must use a new if statement for each thread ID
        {
                begin_f_loop (f,t)
                {
                        // Calculate the area of the face0.00
                        F_AREA(A,f,t);
```

```
                area=NV_MAG(A);
                // Calculate the volume of adjacent cell
                vol=C_VOLUME(F_C0(f,t),THREAD_T0(t));
                C_UDMI(F_C0(f,t),THREAD_T0(t),0)=area/vol;
            }
            end_f_loop(f,t)
        }
        /* else if (t_ID==30) //filter surface ID
        {
            begin_f_loop (f,t);
            {
                // Calculate the area of the face0.00
                F_AREA(A,f,t);
                area=NV_MAG(A);
                // Calculate the volume of adjacent cell
                vol=C_VOLUME(F_C0(f,t),THREAD_T0(t));
                C_UDMI(F_C0(f,t),THREAD_T0(t),0)=area/vol;
            }
            end_f_loop(f,t)
        } */
}
```

```
        printf("all memories are reset to zero, cell on the specified wall isreset to %f\n",
vol/area);
}
DEFINE_SOURCE(BUTYRIC_source, c, t, dS, eqn)
{
        real source;
        real C_butyric, rate1, Irrad;
        C_butyric=C_YI(c,t,0)*C_R(c,t)*10e6; //C in mg/m3
        Irrad=C_DO(c,t); //I in W/m2 (Adjusting as I on catalyst surface changes)
        rate1=(a*Irrad/(1+b*Irrad+e*C_butyric)*C_butyric);  //rate in kmol/m3-system/s
        C_UDMI(c,t,1)=(0.0216/0.361)*C_UDMI(c,t,0)*rate1*0.5;  //rate in kmol/m3-cell/s
        C_UDMI(c,t,2)=Irrad;
        source=-C_UDMI(c,t,1)*88.11; //source in kg/m3/s
        //source=C_ch2o*(-rate1);
        return source;
}

DEFINE_SOURCE(O2_source, c, t, dS, eqn)
{
        real source;
        //C_ch2o=C_YI(c,t,0);
```

```
        //rate1=C_ch2o*K1/(1+K2);
        source=C_UDMI(c,t,1)*32*-5;
        return source;
}

DEFINE_SOURCE(CO2_source, c, t, dS, eqn)
{
        real source;
        //C_ch2o=C_YI(c,t,0);
        //rate1=C_R(c,t)*C_ch2o*29/30*K1/(1+K2);
        source=4*C_UDMI(c,t,1)*44;
        return source;
}

DEFINE_SOURCE(H2O_source, c, t, dS, eqn)
{
        real source;
        //C_ch2o=C_YI(c,t,0);
        //rate1=C_R(c,t)*C_ch2o*29/30*K1/(1+K2);
        source=4*C_UDMI(c,t,1)*18;
        return source;
```

```
}


DEFINE_PROPERTY(Absorption_coefficient,c,t)
{
        real abs_coeff;


        abs_coeff=41.77*C_YI(c,t,0)+3e-17;
}
```

Appendix D: UV Absorption Test

A sample of air saturated with butyric acid was tested to determine if the absorption coefficient of air changes as the concentration of butyric acid decreases.

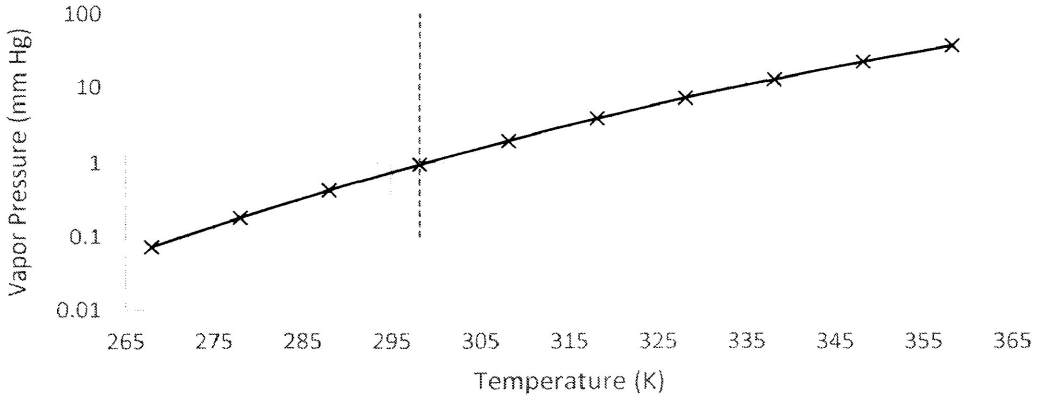

Figure 30: Vapor pressure of butyric acid vs Temperature

Figure 30 was used to determine the vapor pressure of butyric acid at room temperature (25^0C). From the vapor pressure it was determined that the mass fraction of butyric acid in the air was 0.001245 kg/kg.

Using a UV-vis spectrophotometer the absorbance of the saturated air sample was measured every hour in order to obtain an average. For $\lambda = 365$ nm the average absorbance is 0.0158.

Table 3: UV absorbance test data

Time (h)	Absorbance (% transmittance)	λ (nm)
0	0.005527	365.0189
1	0.014665	365.0306
2	0.015072	365.0029
3	0.015157	365.0003
4	0.015844	365.0152
5	0.0158193	365.0078
6	0.015935	365.0109

Using the equation for absorbance the absorption coefficient for air saturated with butyric acid was calculated:

$$A = \alpha L P_x \tag{32}$$

where A is the absorbance, α is the absorption coefficient (atm/cm), L is the path length (10 cm), and P_X is the partial pressure (atm). Fluent requires that α have the unit m^{-1}, so, the equation can be rearranged with concentration written in terms of mass fraction;

$$\alpha = \frac{A}{L\, y_i} \tag{33}$$

According to equation 33 the absorption coefficient would be changing linearly with concentration so a linear curve was created to estimate the absorption coefficient for air containing butyric acid (see Figure 31).

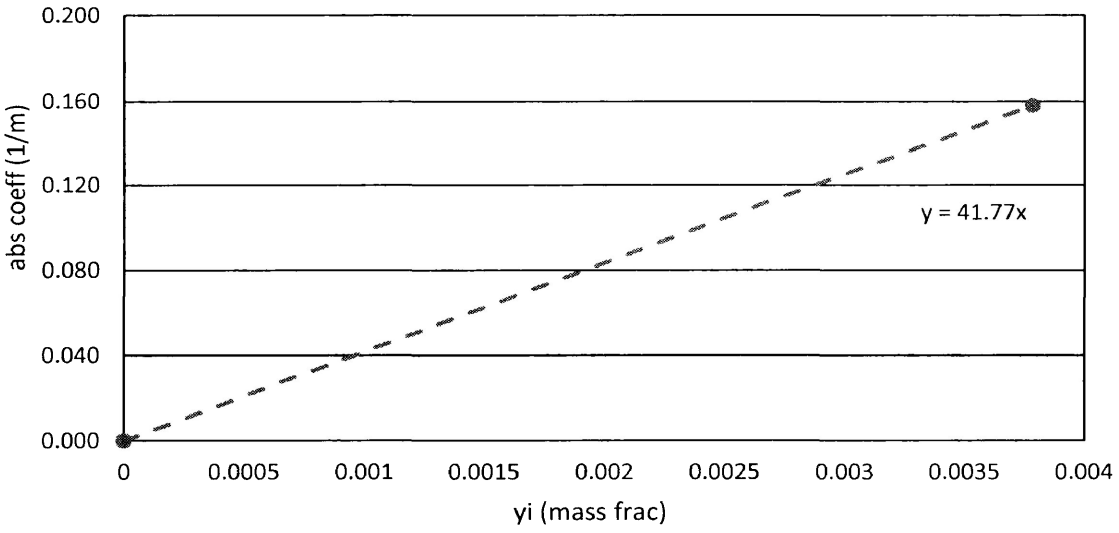

Figure 31: Absorption coefficient vs mass fraction

Appendix E: Overview of Langmuir – Hinshelwood Kinetic Model

Mo, et al (2009) provides a detailed overview of the PCO kinetic theory and the experimental work done. They provided the following approach to describing the surface chemistry of the PCO mechanism:

For a general reactant, R, degrades to produce products A and B has the following stoichiometry:

$$R + O_2 \xrightarrow{TiO_2, h\nu} A + B \tag{34}$$

The rate of change of each of the species can be written as:

$$r = -\frac{d[R]}{dt} = -\frac{d[O_2]}{dt} = \frac{d[A]}{dt} = \frac{d[B]}{dt} \tag{35}$$

Reaction rates are commonly expressed using the power law, where n is 0:

$$r = -\frac{d[R]}{dt} = k[R]^n \tag{36}$$

The PCO reaction involves the adsorption of the reactants prior to undergoing the surface reaction and so the adsorption isotherms will play a key role in the reported kinetic models. The Langmuir-Hinshelwood (L-H) mechanism is the most commonly used method. This mechanism includes the reaction occurring between both the reactant, R, and the oxidizing agent at their adsorption equilibrium.

$$r = k\theta_R\theta_{O_{2,ads}} \tag{37}$$

Where k is the reaction constant which is dependent on temperature and UV intensity, θ_R is the fractional coverage of R adsorbed onto the catalyst surface, and $\theta_{O_{2,ads}}$ is the fraction of oxygen adsorbed onto the catalyst surface.

The L-H model uses the following equation to define θ_R:

$$\theta_R = \frac{q}{q_S} = \frac{m}{m_{max}} = \frac{K[R]}{1+K[R]} \tag{38}$$

where q is the total number of adsorption sites per unit volume of catalyst and q is the number of adsorption sites occupied by R per unit volume of catalyst, m is the amount of R adsorbed per unit volume of catalyst, m_{max} is the maximum amount of R adsorbed per unit catalyst, and K is the adsorption equilibrium coefficient.

A similar equation can also be written for $\theta_{O_{2,ads}}$ where the variables are in terms of the adsorbed oxygen instead of R. However, with the concentration of oxygen in the air being so high in comparison to the concentration of the R, $\theta_{O_{2,ads}}$ is approximately equal to 1. So, the reaction rate can be reduced to:

$$r = k\theta_R = k\left(\frac{K[R]}{1+K[R]}\right) \tag{39}$$

Table 4 is a summary of the results from the studies Mo (2009) reviewed which used the L-H kinetic model to derive the reaction kinetics.

Table 4: Kinetic parameters of unimolecular L – H model of various pollutants

tants	Photocatalyst	VOC conc. (ppm)	PW (nm) / I (mW/cm^2)	T(°C)/ RH (%)	Kinetic parameters		Ref
aldehyde	STS-21 sol	30 – 2000	365/ 1.0	20/40	0.19 μmol/min	0.51 μmol/L	Noguchi and Fujishima, 1998
	P25	1.8	254/ 0.083	24/47	1.48 μmol/ m^2-s	0.94 $ppmv^{-1}$	Yang et al., 2007
aldehyde	STS-21 sol	30 - 2000	365/1.0	20/40	0.16 μmol/min	0.21 μmol/L	Noguchi and Fujishima, 1998
	TiO_2/SiO_2	3000 –	300 – 400/ -	67/-	$3.89x10^{-4}$ L/ g-min	21.9 L/mol	Obuchi et al., 1999
	Pt-TiO_2/SiO_2	6200	300 – 400/ -	67/-	$5.97x10^{-4}$ L/ g-min	36.9 L/mol	Obuchi et al., 1999
		3000 - 6200					
one	P25	590	365/ -	50/23	14.68 g/ m^3-min	0.35 m^3/g	Alberici and Jardim, 1997
	TiO_2/ZrO_2	143 - 1652	365/ 2.3-3.1	30/0	0.097 μmol/$L_{cat.rings}$ -s	0.51 L/μmol	Zorn et al., 1999
ene	TiO_2/Sr_2CeO_4	117 – 308	254/ -	39-60/-	0.0064 mg/L	9.2078 L/mg	Zhong et al., 2007
	P25	0.56 – 1.3	254/ 0.56	25-27/40	1.56 mol/ m^2-s	0.77 m^3/mg	Zhang et al., 2007
ene	P25	5.2 – 26	254/ -	20/45-50	13.388 mg/m^3-s	0.0049 m^3/mg	Bouzaza et al., 2006
	P25	1.2 – 7.2	254/ 0.56	25-27/40	6.77 mol/ m^2-s	0.24 m^3/mg	Zhang et al., 2007
	P25	50 mTorr	356/ 5.3	20.8/2.69	101 μ/ m^2-s	0.022 m/Torr	Jacoby et al., 1995
	P25	538	365/ -	50/23	28.05 g/ m^3-min	0.21 m^3/g	Alberici and Jardim, 1997
	P25	3.7 – 18.5	254/ -	20/45-50	729.254 mg/ m^3-s	0.0017 m^3/mg	Bouzaza et al., 2006
ne	P25	8.7 – 41.4	254/ -	20/45-50	27.461 mg/ m^3-s	0.0199 m^3/mg	Bouzaza et al., 2006
ionic acid	TiO_2 Millenium PC500	–	365/4	30/50	2.02 – 2.10 mmol/m^3-s	0.41-0.32 m^3/mmol	Biard et al., 2007
ric acid	TiO_2 Millenium PC500	–	365/4	30/50	1.98-2.25 mmol/ m^3-s	0.39-0.24 m^3/mmol	Biard et al., 2007

Appendix F: Rectangular Duct Sizing

Common rectangular duct sizes used for air handling ventilation systems (The Engineering Toolbox, 2014):

Table 5: Rectangular duct sizing

Width (mm)	Height *(mm)*										
	100	150	200	250	300	400	500	600	800	1000	1200
200	1)	1)	2)	3)	3)	3)	3)	3)	3)	3)	3)
250	2)	2)	2)	2)	3)	3)	3)	3)	3)	3)	3)
300	1)	1)	1)	2)	2)	3)	3)	3)	3)	3)	3)
400	1)	1)	1)	2)	1)	2)	3)	3)	3)	3)	3)
500	3)	1)	1)	2)	1)	1)	2)	3)	3)	3)	3)
600	3)	1)	1)	2)	1)	1)	1)	2)	3)	3)	3)
800	3)	3)	1)	2)	1)	1)	1)	1)	2)	3)	3)
1000	3)	3)	3)	2)	1)	1)	1)	1)	1)	2)	3)
1200	3)	3)	3)	3)	1)	1)	1)	1)	1)	1)	2)
1400	3)	3)	3)	3)	3)	2)	2)	2)	2)	2)	2)
1600	3)	3)	3)	3)	3)	1)	1)	1)	1)	1)	1)
1800	3)	3)	3)	3)	3)	3)	2)	2)	2)	2)	2)
2000	3)	3)	3)	3)	3)	3)	3)	3)	1)	1)	1)

[1)] Preferred, [2)] Acceptable, [3)] Not common

Figure 32 is used to select an appropriate air velocity through a rectangular duct based on the dimensions (The Engineering Toolbox, 2014).

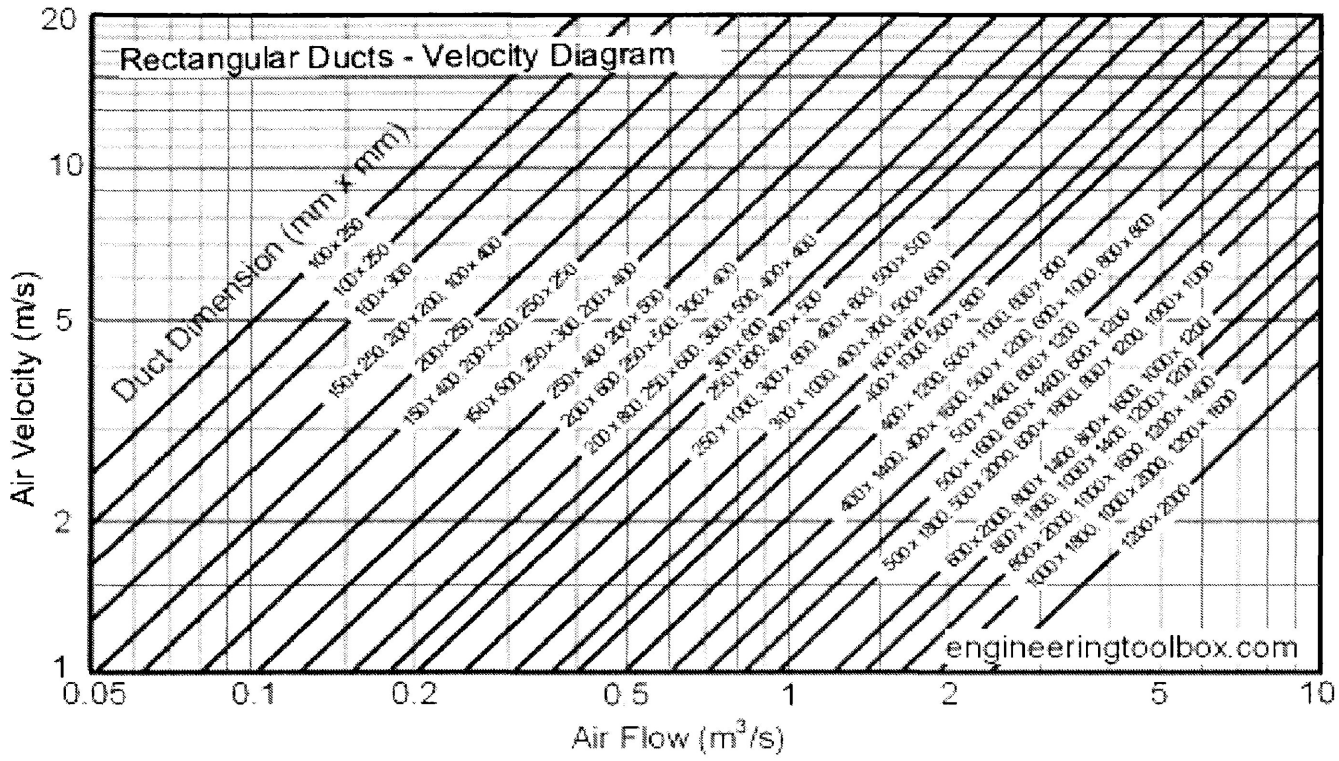

Figure 32: Diagram of recommended air velocities for rectangular air ducts